Microstructures and crystallographic preferred orientation of anorthosites from Oman ophiolite and the dynamics of melt lenses

Luis Morales, Françoise Boudier, Adolphe Nicolas

Microstructures and crystallographic preferred orientation of anorthosites from Oman ophiolite and the dynamics of melt lenses

Luiz F. G. Morales,[1,2] Françoise Boudier,[1] and Adolphe Nicolas[1]

Received 23 February 2010; revised 5 January 2011; accepted 14 January 2011; published 15 April 2011.

[1] Microstructures and crystallographic preferred orientation (CPO) of anorthosite samples interlayered in the upper and lower gabbro sections in the Oman ophiolite were analyzed in this paper. In the anorthosites registering the dynamics of the melt lenses, foliation is flat lying and starts to develop a few meters below the root zone of the sheeted dike complex (RZSDC). Microstructures and CPO of these rocks were developed in response to four different mechanisms: (1) density-controlled settling of plagioclase on the lens floor, (2) deposition of anorthosites related to convection currents, (3) melt compaction, and (4) uncompacted melt accumulation. In these anorthosites, the poles to (010) of plagioclase are parallel to the flow plane of convection, whereas the [100] axes and poles to (001) express the convection flow direction and the axis of convection rolls, respectively. The effect of subsidence of melt lens floor is recorded immediately below the RZSDC and is characterized by the rapid (but progressive) development of dipping foliation and lineation, reflecting the increase of deformation downsection. The degree of foliation and CPO development in the anorthosites is directly related to the distance of the center of the melt lenses before the subsidence starts. Despite the uncertain origin of the anorthosites from the lower gabbro section, all the samples lost the magmatic microstructural characteristics and presently are reequilibrated aggregates. However, they still preserve plagioclase CPO, where some of these patterns present similarities with the anorthosites from the upper gabbro section, but no evidence of intracrystalline deformation under high temperatures.

Citation: Morales, L. F. G., F. Boudier, and A. Nicolas (2011), Microstructures and crystallographic preferred orientation of anorthosites from Oman ophiolite and the dynamics of melt lenses, *Tectonics*, *30*, TC2011, doi:10.1029/2010TC002697.

1. Introduction

[2] Anorthosites have been largely described as an important component of the mafic layering in layered intrusions [e.g., *Irvine*, 1987; *Boudreau*, 1987]. However, this lithology is rarely mentioned as a component of the gabbro section of the oceanic crust, as represented in ophiolites of Oman [*Pallister and Hopson*, 1981] or Bay of Island [*Bédard*, 1991], and just in the last few years it has been receiving some attention [*Nicolas and Boudier*, 2011]. In fact, anorthosites layers and lenses of variable scales are an important component of the lower layered gabbro section at least in the case of fast spreading ridges situation, such as the Oman ophiolite [*Lamoureux*, 1999] or the East Pacific Rise [*Kent et al.*, 1994]. As described by *Boudier et al.* [1996], pure anorthosite bands may form the upper level of graded layers in the lower gabbros in the Oman ophiolite. In addition, recent detailed mapping in the shallow part of the gabbro section of the Oman ophiolite has also pointed out the importance of anorthosites as component of the upper gabbro section, usually as thin lenses within the gabbro foliation, and the possibility to use their occurrence as a key to understand the dynamics of the perched melt lens above the axial magma chamber and the process of subsidence in the axial magma chamber [e.g., *Nicolas et al.*, 2009].

[3] The process of magmatic chamber subsidence [*Nicolas et al.*, 2009] was demonstrated by a high-resolution structural mapping starting from the root zone of the sheeted dikes complex (RZSDC) toward the limit between crustal and mantle rocks in the Oman ophiolite (Figure 1). Most of the sections in the gabbros beneath the melt lens floor display a discordant and steep magmatic foliation parallel to the sheeted dike complex and appear within ten to a few tens of meters below the RZSDC (Figure 2). The steep foliation is traced downward in the foliated upper gabbros over 1 to 1.5 km below to the root zone of the sheeted dikes complex, before progressively rotating into the flat-lying and layered lower gabbros. A second group of sections exhibits gabbros with flat-lying foliations immediately below and parallel to the contact with the RZSDC.

[1]Géosciences Montpellier, UMR, CNRS 5243, Université Montpellier 2, Montpellier, France.
[2]Now at Section 3.2, Deutsches GeoForschungsZentrum, Potsdam, Germany.

0278-7407/11/2010TC002697

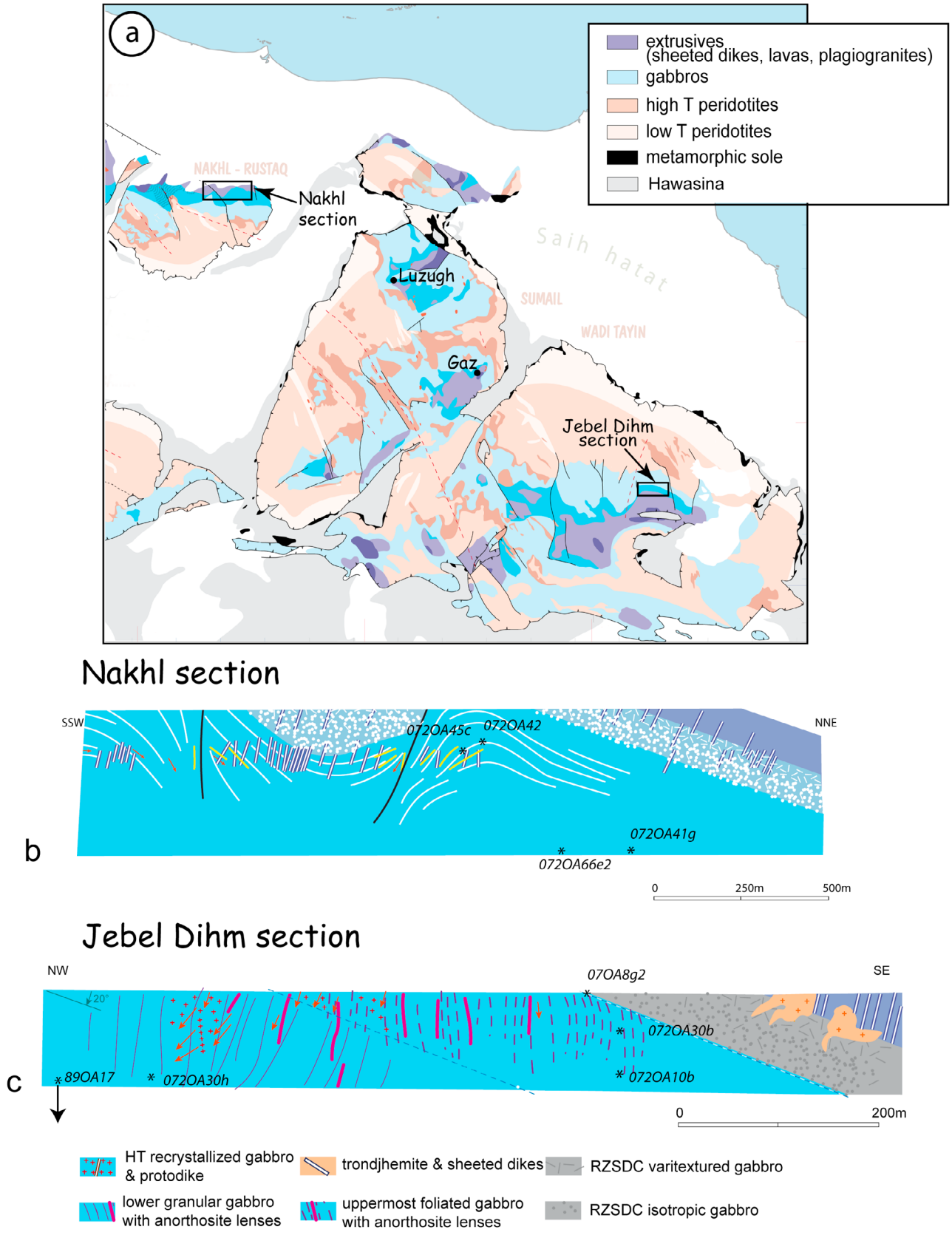

Figure 1. (a) Map of the southern massifs of the Oman ophiolite, with the locations of the cross sections in (b) the East Nakhl and (c) the Jabal Dihm regions showing the approximate location of the samples in relation to the root zone of the sheeted dike complex, where the anorthosites with flat-lying and steep foliations related to dynamic of melt lens and subsidence of the axial magma chamber occur, respectively.

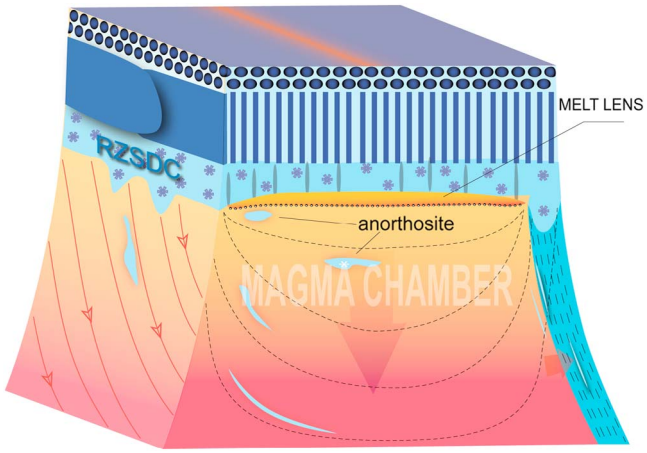

Figure 2. Sketch illustrating the subsidence of the axial magmatic chamber and the location of the melt lenses on the roof of AMC. The subsidence of a crystal mush crystallized on the floor of the melt lenses is subsided and gives origin to the layered gabbros. Dashed lines within the chamber illustrate the trajectory of the anorthosites from the floor of the melt lenses until they reach the magma chamber walls, where anorthosites close to the center of the floor have a longer travel into the AMC during subsidence and are more susceptible to large deformations. Modified after *Nicolas et al.* [2009] (with permission from Elsevier).

[4] Either in the gabbros with vertical foliation or in those that are flat lying, the occurrence of lenses or layers of anorthosites interleaved within the gabbros is ubiquitous, in contrast with the root zone of the dikes, where they are never observed. A special attention has been paid to the occurrence of anorthosites in the upper gabbro section by the fact that, in some places, they occur in swarms that are interpreted as the record of melt supply to the axial melt lens (Figure 3). They are a source of information on the magmatic activity of these lenses. When they are interleaved with steep gabbros, after subsiding and drifting through the wall of the vertical magma chamber (Figure 2), their spacing and dimensions in the field are potential indicators of periodic magmatic influx in the melt lens [*Boudier and Nicolas*, 2011].

[5] Due to their monomineralic character, anorthosites record the evolution of textures controlled by magmatic flow, compaction and recrystallization more clearly than the enclosing gabbros. For this reason, we have conducted a detailed study of microstructures and crystallographic preferred orientations (CPO) in the flat-lying and in the discordant steeply foliated gabbros defined previously, to understand how the anorthosites evolve with depth (from the RZSDC to a couple of hundreds of meters below). Particularly, we address the following questions. (1) What are the mechanisms responsible for the development of different microstructures in the anorthosites of melt lenses? (2) What are the significance of these microstructures in the dynamic and stability of the melt lenses? (3) What is the effect of the deformation related to subsidence in these rocks? By answering these and other questions, we provide more insights about the dynamics of melt lenses and the subsidence of magmatic chambers in fast spreading ridges, complementing the field studies of *Nicolas et al.* [2009] and *Boudier and Nicolas* [2011]. To carry out this work, anorthosite samples representative of the upper gabbro section were selected in different sites from the southern Oman ophiolite (Figure 1). In addition, to test the hypothesis that some of the anorthosites of the lower gabbro section could result from the progressive subsidence of the melt lenses, we also have included in this study some anorthosite samples related to the lower gabbro section with dominant flat-lying foliations due the proximity with Moho.

2. Anorthosites in the Field

2.1. Anorthosites in the Upper Gabbros

[6] In the field, the anorthosites layers can be identified by their light color in relation to the surrounding darker gabbros and by their stronger resistance to erosion (Figure 3). High-resolution mapping starting from the base of the root zone of the sheeted dykes complex (Figure 3) in the southeastern massifs of Oman show that anorthosite lenses just appear immediately below the isotropic gabbros, which in turn lie below the sheeted dikes complex. In addition, the presence of anorthosites marks the starting point for the foliation development in the upper gabbro section. The swarm thickness is 12 m in average (Figures 3 and 4a), and the spacing between them has been estimated to 15 m in average, although it is difficult to estimate with precision due to discontinuity of good exposures along the traverses. In the central area of swarms, there are always one or a few anorthosite layers (Figure 4b) that are much thicker than the surrounding ones. These pure to nearly pure anorthosite layers are in average 40 cm thick, but layers around one meter can also be observed.

[7] The swarms of flat-lying anorthosites have been studied principally in the sections of East Nakhl (Figure 1b). In general, the foliation is horizontal over hundred of meters below the root zone of the sheeted dikes complex. Just a few meters below the bottom of the sheeted dike complex, where the foliation in the anorthosites starts to be developed, the thicker anorthosite layers may contain millimetric oikocrystals of clinopyroxene and ilmenite-magnetite. The foliation is expressed by the dimensional alignment of plagioclase crystals, and a strong shape preferred orientation of plagioclase crystals characterizing the foliation is developed just a few meters below the root zone of the sheeted dike complex. In addition, the anorthosites also display mineral lineations marked by plagioclase and clinopyroxene. Downward in the sections the anorthosites layers tend to become almost pure plagioclase, with clinopyroxene limited to a few tabular-shaped crystals, and oikocrystals progressively disappear. In the Nakhl section, the rotation of the foliation and the superimposed deformation caused by moderate subsidence sometimes is not well defined, but in some places, the foliation can be mildly dipping (Figure 1b). Possible places of melt accumulation are recognized in the field in the form of rounded anorthosite spots of with weak foliation and no lineation associated, with a large number of rounded crystals of clinopyroxene. We draw the attention to the fact that the flat lying anorthosites represent a special case of melt lenses retreating. During the process of "squeezing" of the melt lenses, subhorizontal gabbros and anorthosites are deposited on its floor, and the floor progressively subsides. In this situation, the first anorthosite that appears just

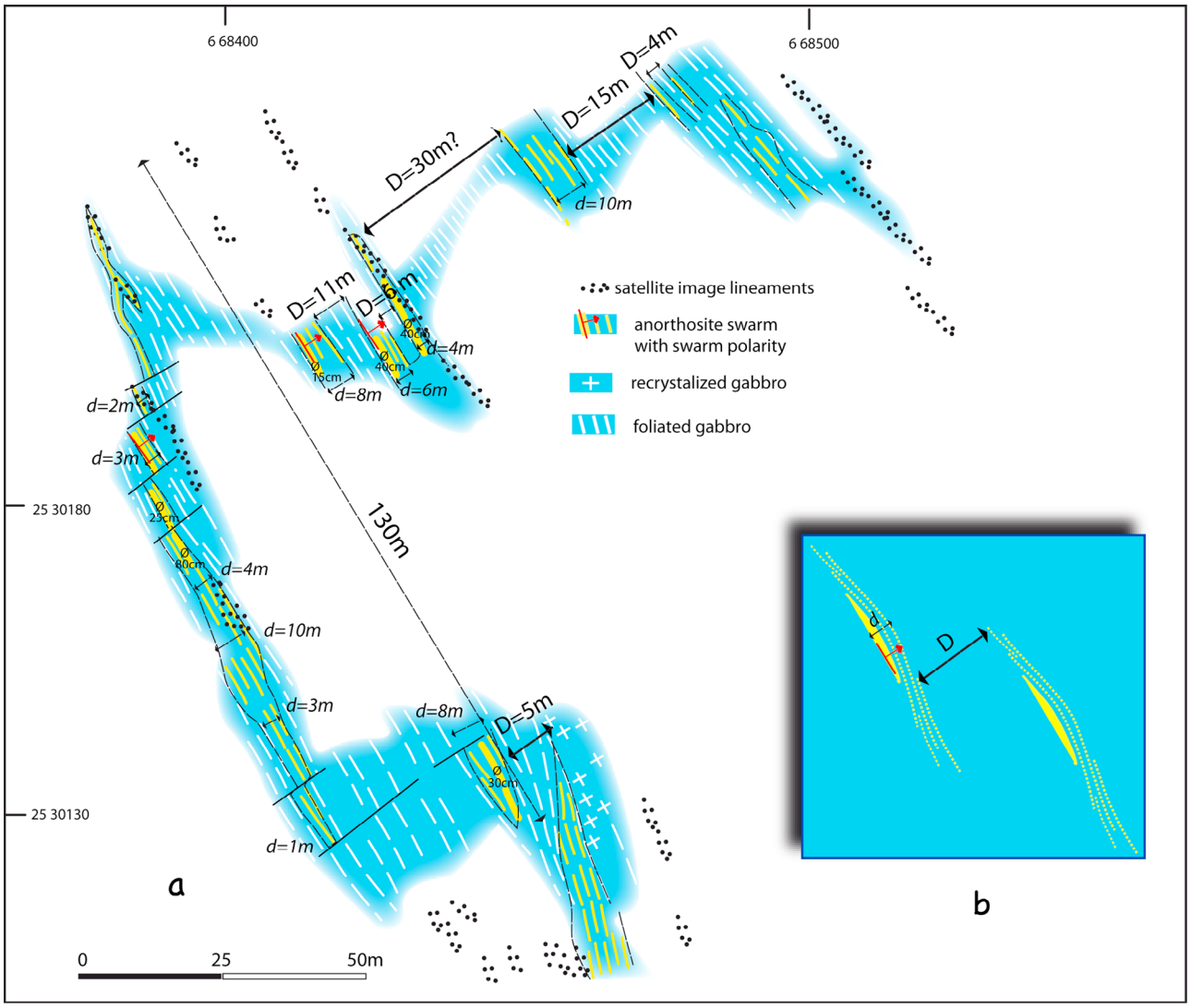

Figure 3. Simplified field map of the anorthosite swarms in the ridge above Wadi Him, in Wadi Tayin massif. This map gives an idea of the thickness of individual layers of anorthosites and the swarms. Details of field measurements can be obtained in the work by *Nicolas and Boudier* [2011].

below the root zone of the sheeted dike complex represents the floor of melt lens margin. On the other hand, deeper anorthosite swarms represent the floor of most internal parts of these lenses (Figure 2).

[8] In Jabal Dihm, the anorthosites are immediately steep, with foliation and lineation developing progressively by the effect of compaction, stretching and shearing downward. Swarms of steep anorthosites were predominantly studied in this area (Figure 2b). They are commonly asymmetrical (Figure 4c), with a sharp base above normal gabbros and a more progressive transition to the overlying gabbros (Figure 4e) and the asymmetry is expressed by the thickness variation in the layers. The swarms commonly occur in the range of only a few meters, and locally isoclinal folds thicken them, before being stretched and sheared during subsidence, where the stretching ratio has been estimated around 2:1. As in the flat-lying anorthosites, the steep anorthosite layers close to the root zone of the sheeted dike complex have oikocrystals of clinopyroxene that rapidly disappear downsection, and the foliation is poorly developed (Figure 4d). Pure anorthosite lenses and layers vary in thickness between thick layers of decimeter scale to a few centimeters (Figure 4d) as in the case of tiger gabbros (Figure 4f). Deeper in the gabbro unit, the vertical foliation developed during the subsidence progressively rotates to a subhorizontal position, becoming parallel to the Moho above the mantle.

2.2. Anorthosites in the Lower Gabbros

[9] The lower gabbros comprise tens of meter thick modally graded sequences. They usually occur as regular layers interleaved with wehrlite bands in the lower part of the section, near the Moho, or as lenticular-shaped foliated gabbros, which are more typical from the upper portion of the lower gabbro section. The anorthosites in the lower gabbros usually occur on the top level of graded layers (Figure 4g), sometimes reaching pure anorthositic composition. In addition, they also occur as intrusive sills parallel or slightly oblique to the gabbro layering and within the thin

lenses in the foliated gabbros. Foliation has shallow dips (15°–20°), it is marked by shape preferred orientation of plagioclase crystals, and usually is parallel to the modal banding observed in the lower gabbros. These anorthosites have also coarser grain sizes and secondary phases such as pyroxene and olivine occur as tabular crystals. Lineations are less visible but they are normally expressed by the alignment of these pyroxenes and (more rarely) by elongated olivine.

3. Methodology

[10] For the study of the microstructures and CPO of the anorthosites of Oman, we have selected 15 representative oriented samples from anorthositic layers and lenses of different thickness collected at different depths (from 0 to 2000 m) in relation to the root zone of the sheeted dike complex. Most of samples were collected in bands parallel or at low angles to the dominant foliation of the host gabbros (Figure 1). Samples were separated in three groups (Table 1): (1) five specimens in flat-lying gabbros, (2) six specimens interlayered in upper gabbros with steep magmatic foliation and (3) four samples of anorthosites of the lower gabbro section, collected at relatively close distances to the Moho. The samples were sectioned normal to the foliation and parallel to the lineation, and also parallel to the foliation. The thin sections were mechanically polished with diamond pastes of grain sizes of up to 1 μm in steps of 30 min in average and by the end, chemically mechanically polished with an alkaline solution of colloidal silica of grain size of 0.03 μm.

[11] Crystallographic preferred orientation of plagioclase were determined via indexation of electron backscattered diffraction (EBSD) patterns in a JEOL JSM 5600 scanning electron microscope (SEM) equipped with an Oxford Instruments/HKL Nordlys EBSD detector and the Channel 5® suite of programs, installed at Géosciences Montpellier (CNRS and Université Montpellier 2). The theory behind this technique is widely described by *Randle* [1992], *Prior et al.* [1999] and *Randle and Engler* [2000] and will not be addressed here. In this paper we make extensive use of the automatic beam mapping of the entire thin sections (~1000 mm^2 of area). The setup parameters for the EBSD analyses were: accelerating voltage of 17 KeV; step size between 40 and 60 μm; working distance of 24 mm; and a spot size of 83. The minimum and maximum number of detected bands on the patterns were four and seven, respectively. All the pole figures were plotted considering a mean angular deviation of 1°. The indexation rate for the raw maps varied between 60 and 80. Postacquisition treatment of EBSD data included the removal of wild spikes, extrapolation of well-indexed points to the zero solutions and elimination of detected grains smaller than three times of the used step size (usually isolated pixels with high MAD numbers). Plagioclase misindexation due a twofold rotation (180°) along ⟨010⟩ and ⟨001⟩ axes, caused by Albite and Carlsbad twinning, respectively, were also correct to avoid errors on grain detection [*Feinberg et al.*, 2006]. To avoid overextrapolation of orientation data due variations on grain sizes, the data was plotted as one point per grain in a common tectonic reference frame for all the samples (E-W vertical foliation; E-W horizontal lineation). The strength of the CPO was characterized by the dimensionless texture J index ($J = \int f(\mathbf{g})^2 d\mathbf{g}$), where $f(\mathbf{g})$ is the orientation distribution function (ODF) and describes the volume fraction of the sample with an orientation $\mathbf{g}$ and $d\mathbf{g}$ [*Bunge*, 1982; *Tommasi et al.*, 2000]. Due the inherent difficulties of calculation of J index in triclinic minerals, we calculated the fabric strength assuming a monoclinic symmetry for the multiplicity of the rotation axis Z. This means that a certain volume of orientations were not considered in the calculations due the smaller dimension of the ODF space for a monoclinic symmetry in relation to the space for triclinic materials. Normally, J index has a value of 1 for a random distribution and infinite to a single crystal, but due the truncation of harmonic series at degree 22 (and considering the monoclinic symmetry), the maximum for plagioclase is around 500.

4. Textures and Microstructures

4.1. Textures in the Upper Gabbros

4.1.1. Anorthosites With Flat-Lying Foliations

[12] Just below the root zone of the sheeted dikes complex, the anorthosites are poorly foliated and usually present poikilitic clinopyroxene (Figure 5a). These rocks contain relatively large plagioclase crystals, where the largest tabular grains may reach dimensions of 1.0 × 0.3 mm thick in a fine-grained matrix, with an average grain dimension of 0.6 × 0.2 mm. In the section normal to the foliation, the orientation of plagioclase crystals is very loose, but characterizes a weak foliation. Most of the crystals present albite twinning, and strong chemical zoning is observed in some crystals near the contact with the root zone of the sheeted dike complex. The weak orientation of plagioclase crystals is confirmed in the section parallel to the foliation (Figure 5b), where no clear orientation is observed and the lineation is not distinct. Rapidly, some 10 m below the sheeted dike complex (Figure 5c), the general texture becomes very anisotropic due to strong magmatic foliation, resembling a fluidal texture. Plagioclase crystals in these rocks possess two dominant dimensions, the first with crystals around 1.0 × 0.3 mm and the second where the tablets reach average dimensions of 2.0 × 0.3 mm. The majority of grains present albite twinning and zoning become more a common feature (An_{80} in the core and An_{60} in the rims). In one of these samples we also observed synneusis microstructures (Figure 5d) in the plagioclases.

Figure 4. (a) Field aspect of the anorthosite swarms, 15 m thick in the East Nakhl section, with (b) decimeter-thick layers of pure anorthosite. (c) When related to the subsidence processes, the anorthosites may occur as deformed lenses within the surrounding gabbros due to stretching and shearing, and (d) when close to the rooted zone of the sheeted dike complex, they may preserve undeformed poikilitic crystals of clinopyroxene, indicating the absence of compaction. Thickness of anorthosite layers may be variable downsection, from (e) decimeter to (f) centimeter scale, in the later case giving a banded aspect to the rock, known as tiger gabbros. (g) In the lower gabbros, anorthosites may occur at the top of the graded sections or as small-scale intrusions oblique or subparallel to the foliation of the surrounding gabbros.

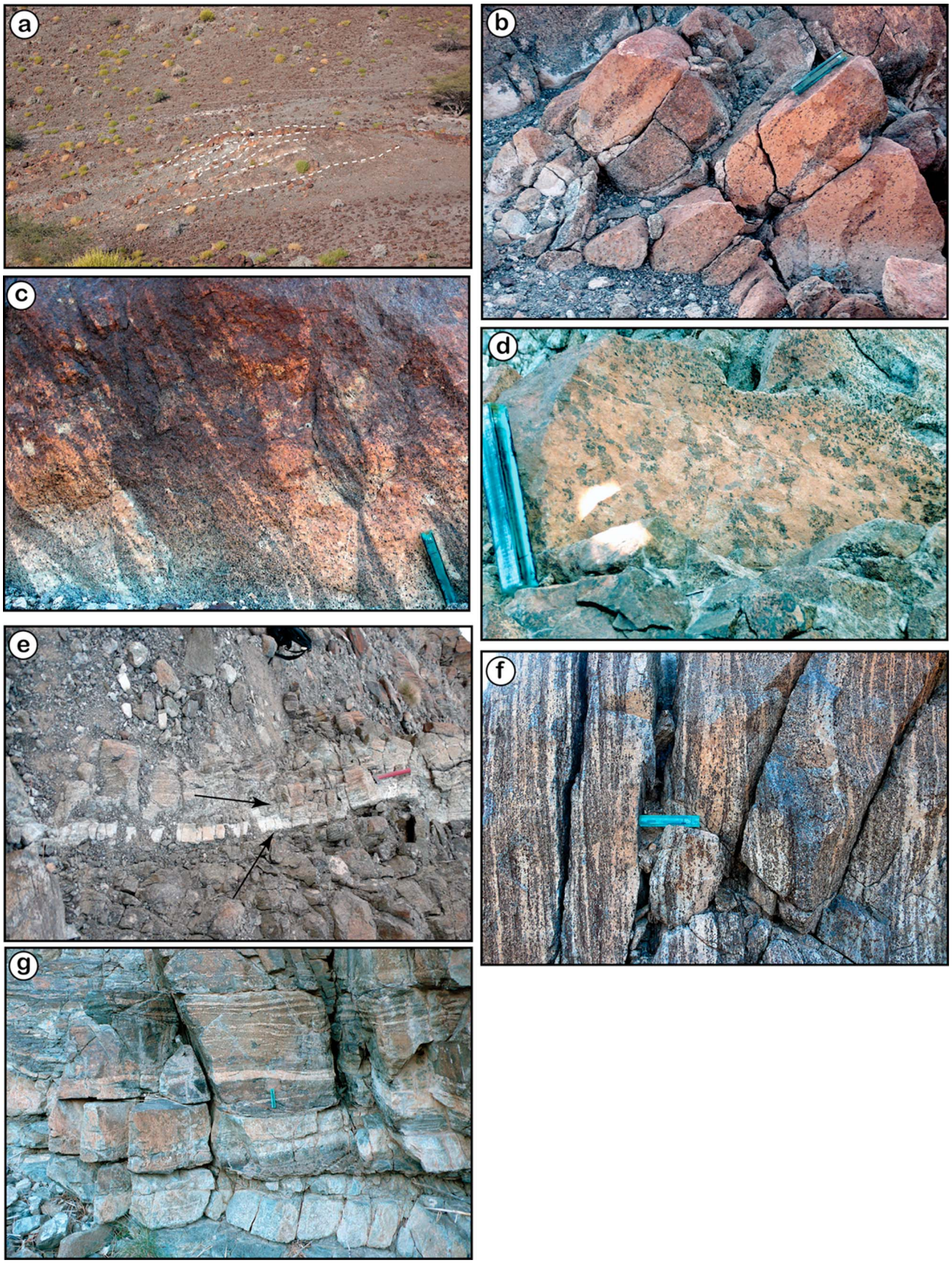

Figure 4

Table 1. Description of the Individual Samples Containing Details About the Vertical Distance From the Rooted Zone of the Sheeted Dike Complex (RZSDC), Occurrence Type, Orientation of Mesostructures in the Field, Main Textures, and Microstructural Quantification Parameters, Including Fabric Strength (J), Grain Size/Aspect Ratio, and Modal Composition Based on the EBSD Maps[a]

Depth	N°	Location	Type	Foliation (S)	Lineation	Orientation[b]	Rotation	J	Texture	μ Probe	Grain Size[c] (mm)	Aspect Ratio[c]	Modal Composition[d] (%)
Upper Crust: Flat-Lying Foliation													
0 m, RZSDC	072OA42	Nakhl	anorth band	110S20	no			2.55	Cpx poikilitic, uncompacted		0.15, 1.0, 0.15 to 0.55	1, 8, 1 to 4.5	89.1, 9.1, 1
10 m	072OA45C3	Nakhl	anorth band, Ø 40 cm	120N10, dip variable		az 75, TS 80°/L	L az 160, rotate 80°	11.91	Pl tabular fluidal, Cpx interst	zoning, An80-59	0.15, 1.2, 0.15 to 0.52	1, 9, 1 to 5	97.3, 1.8, 1
30 m	072OA45C4	Nakhl	gb anorth	120S40	60SW30	az NS 45°/L	L 45 in TS, rotate 45°	7.94	Pl tabular fluidal, Cpx granular	zoning, An79-71	0.15, 1.3, 0.15 to 0.53	1, 12.5, 1 to 5	83.4, 16.6, 0
250 m	072OA41g	Luzugh	anorthosite in spot	120S55	?	L (???) az 60		2.70	ophitic gb		0.15, 1.8, 0.15 to 0.65	1, 11.5, 1 to 4.5	78.3, 15.9, 3.25[e]
300 m	072OA66e2	Al Khod	anorth bed, Ø 5 cm			//L 5N30		9.07	Pl tabular, Cpx, oxydes interst		0.15, 1.5, 0.15 to 0.82	1, 7, 1 to 4	95.1, 4.9, 0
Upper Crust: Steep Foliation													
0 m	07OA8g2	Gaz	anorth band, Ø 15 cm	120S55	60Est55	//L		2.08	slight foliation, Pl tabular		0.15, 1.4, 0.15 to 0.6	1, 6, 1 to 3.8	88.0, 12.0, 0
50 m	072OA30b	Him	anorth band, Ø 5–10 cm	25W70	0N50	//L		3.78	Cpx interst	zoning, An70-57	0.15, 2.8, 0.15 to 0.6	1, 8.5, 1 to 4	98.3, 0, 1.7
90 m	072OA10b	Farah	gb anorth	30W70	145N70	//L 145N70		4.43	Pl tabular fl, Cpx granular	zoning, An81-69	0.15, 2.1, 0.15 to 0.55	1, 7, 1 to 4.2	96.2, 3.0, 1.0
600 m	072OA30h	Him	gb anorth tiger	150Est80	15Est60	//L 15E60		4.93	Pl tabular	zoning, An81-68			93.3, 5.9, 0
750 m	072OA18b	Him	anorth band, Ø 30 cm	140N90	140N40	//L 140N40		8.73		An82	0.15, 1.8, 0.15 to 0.6	1, 10, 1 to 4.5	98.3, 1.7, 0
	072OA18c	Him	tiger gb	140N90	140N40	//L		3.68	Pl tabular	An82-84	0.15, 1.5, 0.15 to 0.6	1, 11.5, 1 to 4.2	97.8, 2.2, 0
Middle to Lower Crust													
1500 m	95OA165a	Abda	Moho	140Est35	60Est35			4.24	crenulated		0.15, 2.5, 0.15 to 0.9	1, 10.5, 1 to 3.5	98.7, 1.3, 0
1500 m	89OA17	Farah		110S45	90W10			7.96	granular	x	0.15, 1.4, 0.15 to 0.65	1, 7.5, 1 to 3.5	91.9, 6.9, 0
2000 m	072OA37	Wariyah	anorth bed	10Est20	50Est10	az 50 //L		4.62	granular	x	0.15, 2.3, 0.15 to 0.75	0.15, 2.3, 0.15 to 0.75	88.9, 11.1, 0
Graded Bedding	072OA37b		anorth de GB			//L		4.03		An85-83	0.15, 2.5, 0.15 to 0.75	1, 8.5, 1 to 3.5	

[a]Grain size and aspect ratio were determined in the orientation maps. Cpx, clinopyroxene; anorth, anorthosite; gb, gabbro; interst, interstitial; az, azimuth; Opx, orthopyroxene; //L, parallel to the lineation. Attitudes of foliations and lineations as measured in the field, in the anorthosites and surrounding gabbros.

[b]Orientation is thin section normal to S.

[c]Value format is min (minimum value of grain size/aspect ratio), max (maximum size/aspect ratio), AI (average interval).

[d]Value format is plagioclase, Cpx, olivine.

[e]Also included is 2.65% orthopyroxene.

Table 2. Chemical Composition of a Plagioclase Crystal From the Sample 07-2-OA-42, Assumed as the Composition of the Anorthositic Magma Used to Calculate the Viscosity Using the Method Introduced by *Giordano et al.* [2008]

	Viscosity
SiO_2	47.57
TiO_2	0.08
Al_2O_3	32.45
FeO (T)	0.5
MnO	0
MgO	0.02
CaO	16.13
Na_2O	2.28
K_2O	0.03
P_2O_5	0.02
H_2O	0
Total	99.08

Synneusis refers to the process of drifting together and mutual attachment of crystals suspended in a melt at early stages of crystallization [*Vance*, 1969]. The crystal bounding usually occur along the faces of lower interfacial energy and in the case of plagioclase, the process result from the coalescence of the two grains along the (010) planes. In the section parallel to the foliation, the orientation is weak, but the alignment of some plagioclase laths defines a lineation that confirms the pyroxene lineation measured in the field. Oikocrystals of clinopyroxene may be slightly flattened or absent, in the case of thicker anorthosite layers. Grain boundaries of plagioclase are predominantly straight and sharp, and curved boundaries were not observed in the anorthosites of the upper part of the section.

[13] At depths of 300 m below the root zone of the sheeted dike complex, foliation is expressed by the strong shape preferred orientation of plagioclase, with average grain dimension of 2.0 × 0.8 mm. Broad magmatic twins are less abundant, while twins oblique to the foliation are still present (Figure 5e). Crystal zoning is completely absent at these depths and grain boundaries are more irregular, with lobate and, more rarely, concave interfaces (Figure 5f). In the anorthosite spots, plagioclase crystals are thicker and aspect ratio decreases significantly, and the crystals may have a more prismatic than tabular shape, when observed in a section parallel to the foliation (Figure 5h). Interstitial crystals of clinopyroxene and altered olivine, filling the spaces between tiled plagioclase crystals, is a common features in these places of melt accumulation even at relatively great depth with respect to the root zone of the sheeted dike complex (Figures 5g and 5h). In these rocks, foliation is weak and grain boundaries are predominantly straight and sharp, and in most places plagioclase appears surrounded by clinopyroxene.

4.1.2. Anorthosites With Steep Foliation at Shallow Levels

[14] Steeply dipping foliated gabbros immediately underlying isotropic gabbro from the RZSDC may contain some thick anorthosite lenses that still include poikilitic clinopyroxene (Figure 6a). These anorthosites are poorly foliated with relatively thick tabular plagioclase, with a grain dimension average of 1.5 × 0.7 mm. The crystals usually present albite twin and are strongly zoned at shallow depths. A few tens of meters below, plagioclase axial ratio increases slightly, and the average grain dimension is about 2.5 × 0.7 mm. Due the relative increase in the aspect ratio of plagioclases and the increase of, foliation becomes stronger (Figure 6b). Down in the section, the foliation becomes more prominent and it is particularly well developed in the particular facies of "tiger gabbros." In these rocks, plagioclase crystals are predominantly tabular with average dimensions of 2.0 × 1.0 mm (Figure 6d). Some crystals of lower aspect ratio may appear crosscutting the foliation and some plagioclase crystals may occur wrapping around granular and (less common) elongated clinopyroxene. The deepest samples are usually well-compacted pure plagioclase rocks, with no interstitial clinopyroxene, but with interstitial spinel. Grain boundaries are predominantly straight and sharp, but slightly curved boundaries can be observed. In these samples, impingements are also observed (Figure 6e). A secondary shape preferred orientation of plagioclase crystals occur cutting the main foliation in the anorthosites, and tiled crystals oblique to the main foliation are common features in both shallow and deep anorthosites (Figure 6f). This has been ascribed as S-C structures developed in melt-poor crystal mushes [*Nicolas and Ildefonse*, 1996].

4.2. Textures in the Lower Gabbros

[15] From the four studied anorthosites, one sample came from a centimeter-thick layer in foliated gabbros (specimen 89-OA-17), and three specimens belong to the top level of a graded section, one sampling a layered gabbro at Moho (95-OA-165a), another sampling a graded bedding (07-2-OA-37b) and the last, an anorthosite sill (07-2-OA-37) (Table 1). These samples are characterized predominantly by restored, equigranular textures with grain dimensions between 1 and 1.5 mm (Figure 6g). Twins are relatively well preserved, but they are absent in a number of grains. Grain boundaries between plagioclase crystals can be either straight or concave, and well equilibrated 120° triple junctions between plagioclase crystals are also be observed

Figure 5. (a) Microstructures on the flat-lying anorthosites right below the root zone of the sheeted dike complex include weak shape preferred orientation of plagioclase crystals marking a weak foliation and poikilitic crystals of clinopyroxene, indicating a limited degree of compaction, (b) with the absence of lineation in a section parallel to the foliation. (c) On the other hand, 10 m below from sheeted dike complex, the foliation expressed by a strong shape preferred orientation of plagioclase is quite strong, resulting in fluidal textures. (d) In addition, synneusis features indicate the turbulent flow of a suspension flow and not of a crystal mush. (e) Down in the section, pure anorthosite bands with strong foliations are developed possibly by melt expulsion from the crystal mush. Magmatic twins progressively disappear, following the appearance of oblique twins (marked by white arrow), which suggests the local activation plastic deformation in plagioclase crystals. (f) Grain boundaries become more irregular, and in a few places on these flat-lying anorthosites, (g and h) plagioclase crystals may have prismatic shapes, as corroborated sections perpendicular to each other.

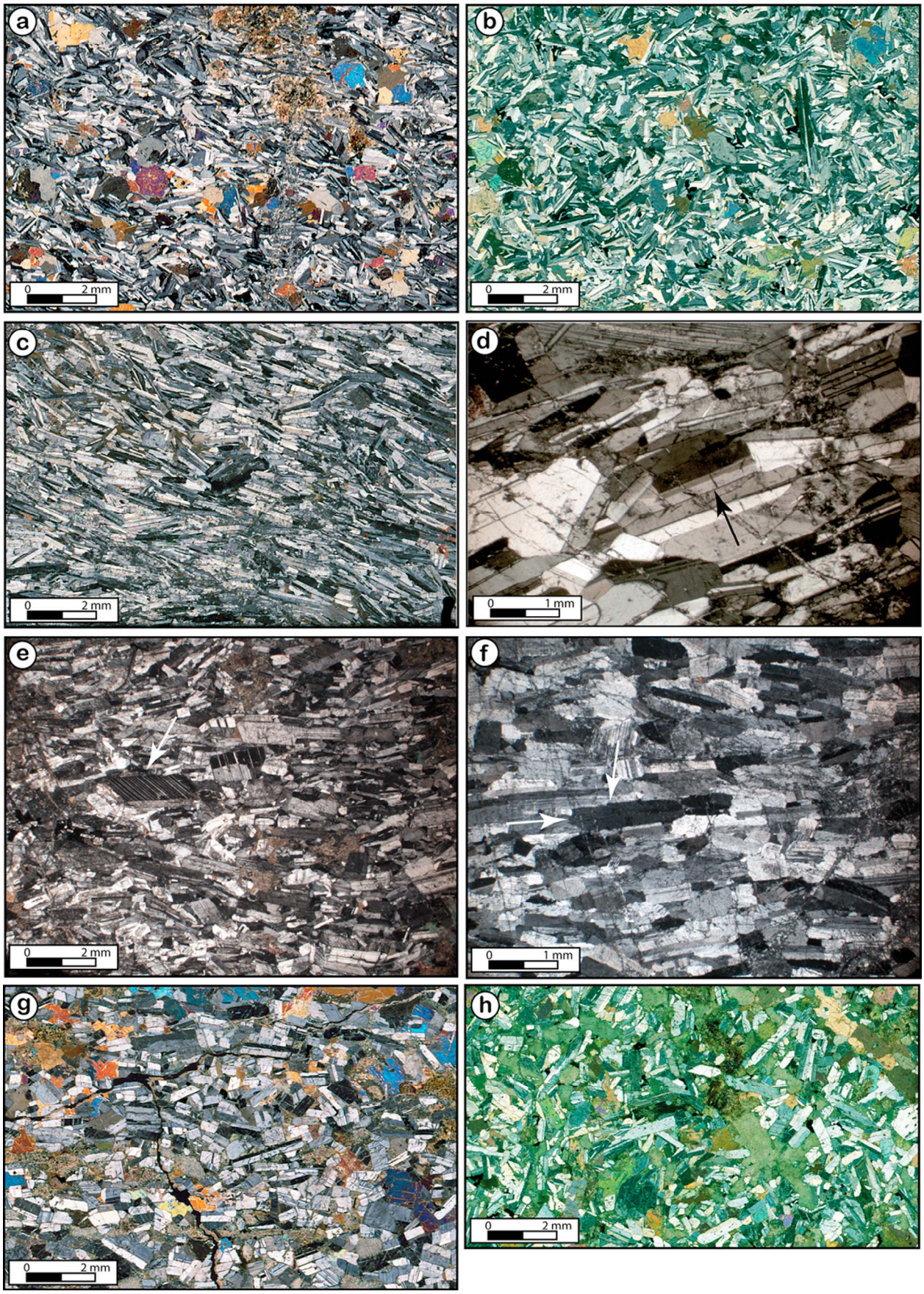

Figure 5

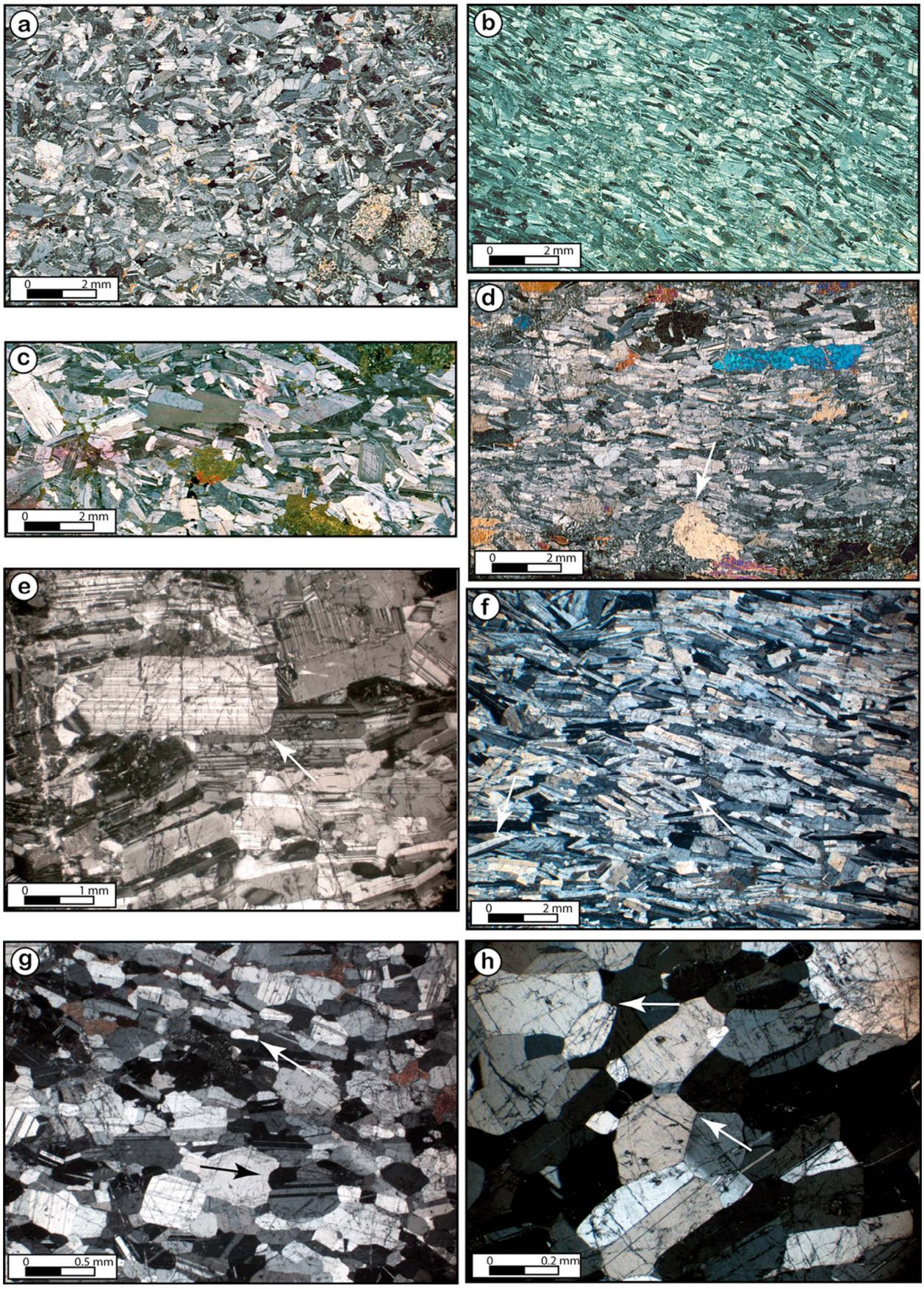

Figure 6

(Figure 6h). Intracrystalline deformation features, such as undulose extinction and subgrain boundaries are normally absent, and the only traces of plastic strain observed in the lower crust anorthosites are limited by pinching twins, saturated and concave grain boundaries (Figure 6g). Except for the last criteria, there is no significant difference between the four samples. Clinopyroxene is predominantly granular and more rarely, tabular, with average aspect ratio of 2:1. In one of the samples, olivine relicts surrounded by chlorite may also occur.

4.3. Plagioclase Aspect Ratios

[16] Visual determination of the aspect ratio of plagioclase crystals in sections parallel to the lineation and normal to the foliation, and also parallel to the foliation, indicate the predominance of three plagioclase shapes. The first, dominant, is represented by elongated tabular crystals with average aspect ratios of 4:2.5:1, reaching in some cases ratios of 8:3:1. These crystals are found in both flat-lying and steep anorthosites and the largest aspect ratio values commonly occur in the flat-lying anorthosites. The second type is represented by prismatic-shaped crystals, with average aspect ratios of 4:1:1, and usually found in places with large amounts of interstitial clinopyroxene, such as in the anorthosite spots. The third shape is represented by tabular crystals with low aspect ratio (2:2:1) and equigranular crystals predominantly found in the lower crustal anorthosites. It is worth to notice that in these deep anorthosites, some crystals that appear "equigranular" in sections parallel to the lineation and normal to the foliation, have a more tabular aspect when observed in sections parallel to the foliation, similarly as demonstrated by *Mainprice and Münch* [1993].

5. Plagioclase CPO

[17] The pole figures were plotted in the tectonic reference frame with the foliation oriented vertically in E-W position (horizontal line), with the lineation lying in a horizontal position, also in E-W direction. The horizontal trace in the center of the pole figures mark the position of foliation in this reference frame, so the pole of the foliation lies in the north of the figures, and it is marked with Z. The lineation position is marked with X. As plagioclase is a triclinic mineral, the complete representation of the CPO is given by the pole figures of [100] axis and the poles to (010) and (001) planes, because the axes [010] and [001] do not make right angles with the respective planes. The plagioclase CPO is characterized by the alignment of the poles to (010) planes parallel the pole of the foliation in all the specimens (Figures 7 and 8). In both situations, the [100] axes are distributed along continuous single girdles parallel to the foliation, with the tendency of a maximum concentration parallel to the lineation or parallel to Y (in exceptional cases) on the tectonic reference frame. These characteristics, in addition to the lack of obliquity of the CPO relative to the macroscopic structures (foliation/lineation), corroborate the magmatic character expressed by the textures. The poles of (001) planes are distributed in two different forms, which are directly related to the shape of plagioclase crystals. Predominantly the poles of (001) are distributed along continuous single girdles parallel to the foliation, reflecting the tabular aspect of the plagioclase crystals. However, some samples have the (001) planes of plagioclase also parallel to the foliation, meaning that they have similar distribution patterns (010) planes (Figures 5g and 5h and 7d, specimen 07-2-OA-41g). This abnormal distribution of the poles of (001) reflects a more prismatic shape of the plagioclase crystals. This configuration allows a rotation around [100] and the consequent interchange between the poles of (010) and (001) parallel to Z in the reference frame.

[18] Predominantly, the CPO of (010) is stronger in the subhorizontal anorthosites than in the steep-dipping ones, and the girdles of [010] axes and poles to (001) are also sharper in the anorthosites related to the melt lenses. With increasing in depth in relation to the root zone of the sheeted dike complex, the plagioclase CPO becomes quite strong. The maximum concentration of poles to (010) varies from 4% right below the sheeted dike complex, to 13% just 10 m below, which is accompanied by an increase in the J index from ~2 to 12. The CPO remains stable down in the section, and at depths of 300 m, the CPO patterns are essentially the same, with a slight variation in the J index (Figure 7e). We also noticed that after the acquisition of the strong CPO, the maximum of [100] axes is relatively stable throughout the pole figures.

[19] The CPO of the anorthosites with steep foliation exhibit a more progressive evolution with depth compared to flat-lying ones. The pole figures in Figures 8a–8f show a progressive increase of concentration of poles to (010) parallel to the pole of the foliation with increasing depths, with the maximum concentration varying from 3 to 12% between 0 to 750 m in relation to the root zone of the sheeted dike complex. This variation follows the increase of J index from ~2 to almost 9 at same depths. Again, the concentration of [100] axes is relatively stable after the acquisition of the CPO, but the concentration of poles to (001) is weaker in the steeply foliated compared to the flat-lying anorthosites.

[20] Most of the samples of the lower crustal anorthosites are representative of the layered section, and the only exception is the specimen 89-OA-17, that came from a centimeter layer in a foliated gabbro (Figure 8h). In the

Figure 6. (a) Microstructures in steeply dipping anorthosites right below the root zone of the sheeted dike complex may contain relatively large poikilitic crystals of clinopyroxene, and the anorthosites are poorly foliated. (b) Around 50 m below the sheeted dike complex, the foliation becomes quite strong, (c) and a lineation is also well marked in a section parallel to the foliation, where some crystals possibly have prismatic shape. (d) Plagioclase crystals wrapping around granular clinopyroxene crystals may occur in the tiger gabbro facies. (e) Impingements along crystal boundaries of plagioclase are also observed. (f) Tiled crystals oblique to the main foliation plane of these rocks are also observed. (g) The textures of lower crustal anorthosites are characterized by an equigranular, restored aspect, with magmatic twins nearly absent, and grain boundaries varying from straight and sharp to strongly curved. (h) The presence of 120° triple junctions in well-equilibrated grain boundaries is also a strong characteristic of these anorthosites.

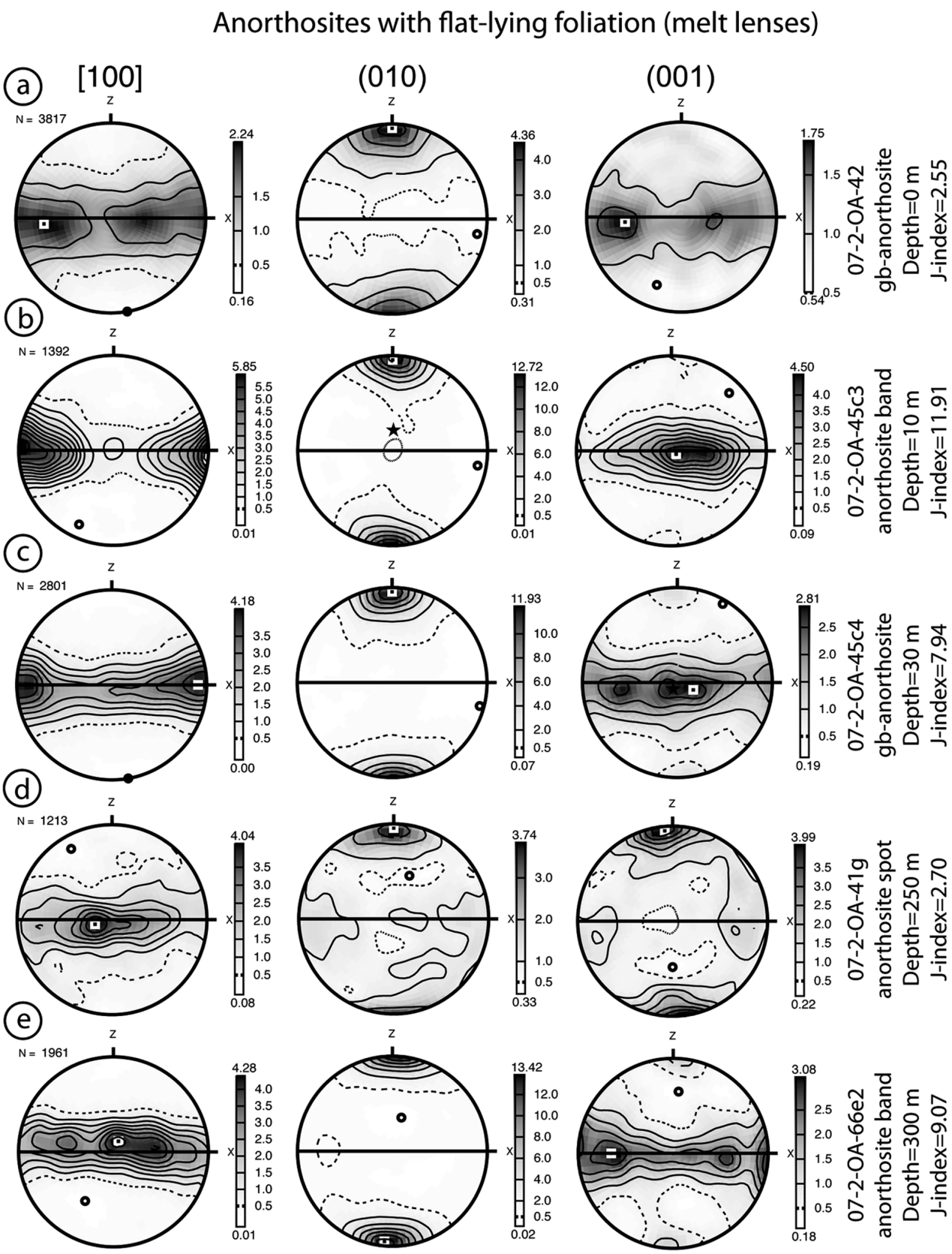

Figure 7. (a–e) Crystallographic preferred orientation of plagioclase of the flat-lying anorthosites, for [100] axes and the poles to (010) and (001) planes. Pole figures plotted in the tectonic reference frame, with the vertical foliation aligned in the direction E-W and horizontal lineation also aligned in the E-W. Lower hemisphere, equal-area net, multiples of uniform distribution, MAD < 1.3°, inverse-log color scale.

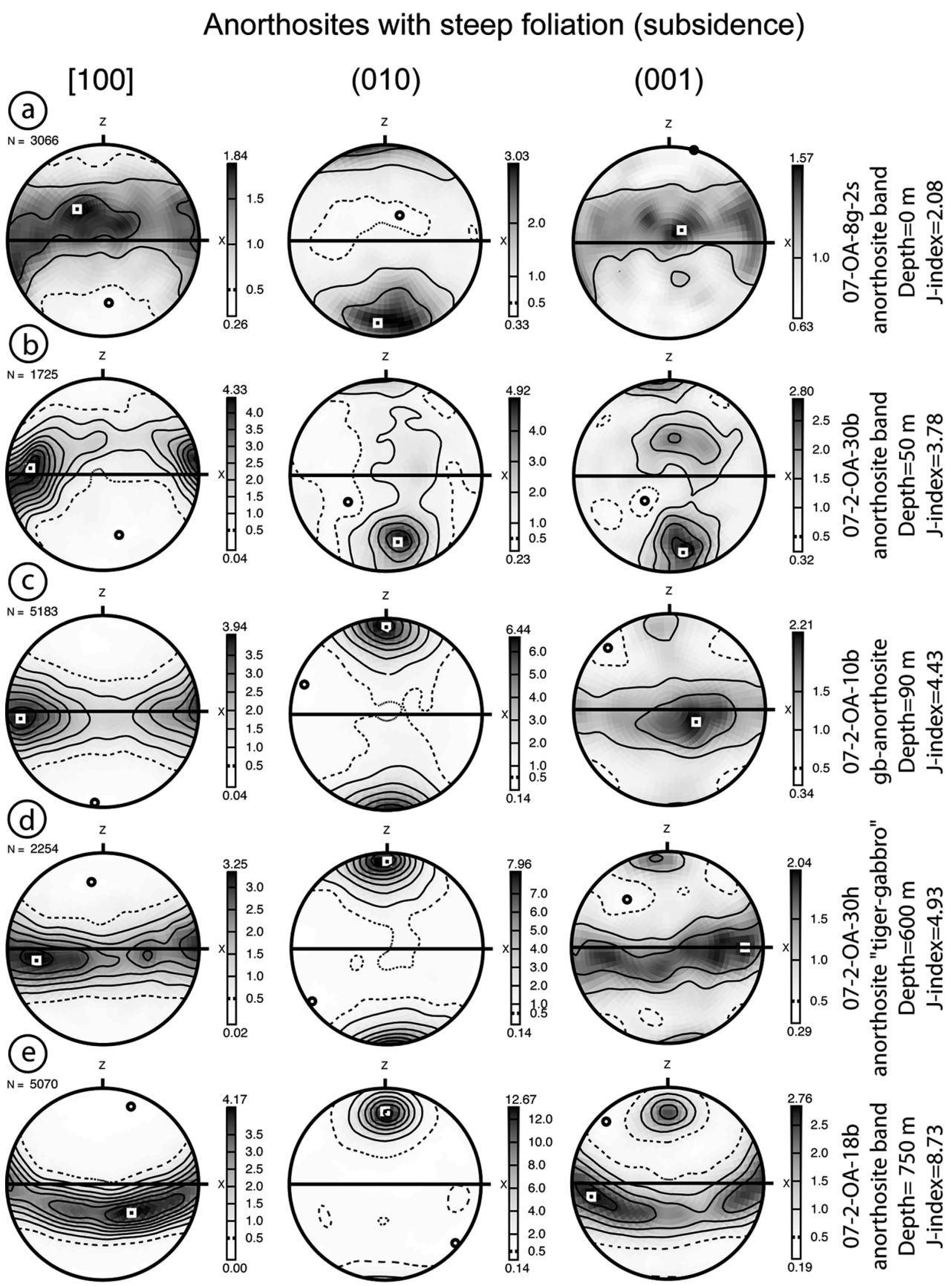
Anorthosites with steep foliation (subsidence)
[100]
(010)
(001)
a
N = 3066
1.84
1.5
1.0
0.5
0.26
3.03
2.0
1.0
0.5
0.33
1.57
1.0
0.63
07-OA-8g-2s
anorthosite band
Depth=0 m
J-index=2.08
b
N = 1725
4.33
4.0
3.5
3.0
2.5
2.0
1.5
1.0
0.5
0.04
4.92
4.0
3.0
2.0
1.0
0.5
0.23
2.80
2.5
2.0
1.5
1.0
0.5
0.32
07-2-OA-30b
anorthosite band
Depth=50 m
J-index=3.78
c
N = 5183
3.94
3.5
3.0
2.5
2.0
1.5
1.0
0.5
0.04
6.44
6.0
5.0
4.0
3.0
2.0
1.0
0.5
0.14
2.21
1.5
1.0
0.5
0.34
07-2-OA-10b
gb-anorthosite
Depth=90 m
J-index=4.43
d
N = 2254
3.25
3.0
2.5
2.0
1.5
1.0
0.5
0.02
7.96
7.0
6.0
5.0
4.0
3.0
2.0
1.0
0.5
0.14
2.04
1.5
1.0
0.5
0.29
07-2-OA-30h
anorthosite "tiger-gabbro"
Depth=600 m
J-index=4.93
e
N = 5070
4.17
3.5
3.0
2.5
2.0
1.5
1.0
0.5
0.00
12.67
12.0
10.0
8.0
6.0
4.0
2.0
0.5
0.14
2.76
2.5
2.0
1.5
1.0
0.5
0.19
07-2-OA-18b
anorthosite band
Depth= 750 m
J-index=8.73

Figure 8

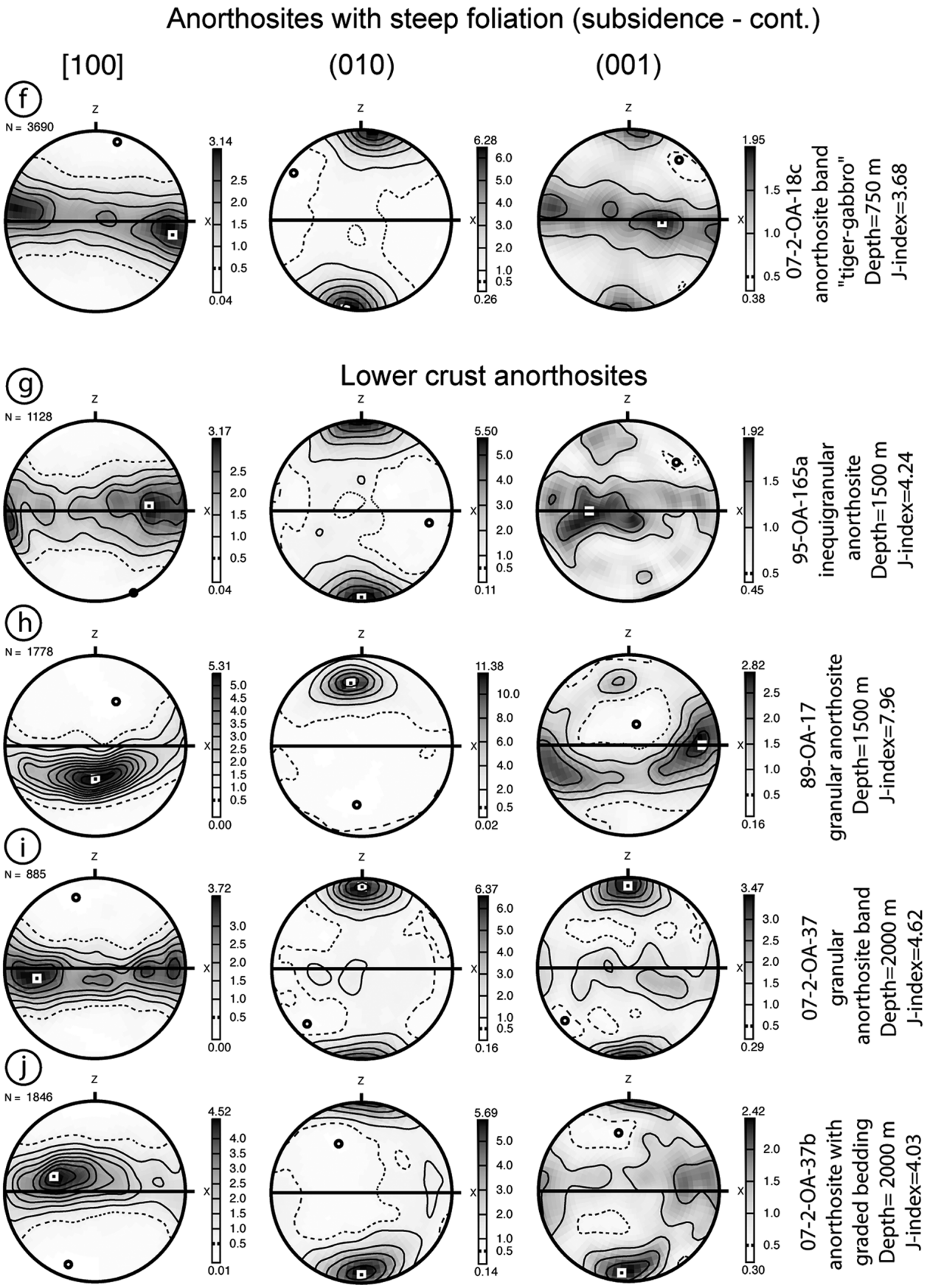

Figure 8. (continued)

layered gabbro anorthosites (Figures 8g, 8i and 8j), the (010) planes are parallel to the foliation, the [100] axes are distributed in a girdle along the foliation and the poles to (001) can be distributed either as a girdle parallel to the foliation or form a maximum in Z.

6. Discussion

6.1. Origin of the Melt Lenses

[21] The melt lens can be classified in stable and unstable end-members. In the stable lenses, melt feeding is constant and abundant, and the feeding of these lenses is accompanied by the progressive subsidence of the floors and the magma chamber. Unstable melt lenses refer to the lenses that receive reduced melt refilling and tend to shrink. During the retreating process and consequent decreasing on the dimensions of the lens, the anorthosite layers settled on its floor enter in contact with hydrothermal circulation and solidify. The irregular spacing between the swarms as observed in the field suggests that the feeding of the melt lenses with basaltic magmas was episodic [*Boudier and Nicolas*, 2011]. The presence of small crystals of plagioclase as inclusions in clinopyroxene and olivine, and the repetition in the field of anorthosite layers grading to gabbros, indicate that plagioclase was the first phase to crystallize from the new melt injections. As illustrated by the triangular phase diagram of *Morse* [1980] describing the crystallization of forsterite-diopside-anorthite, olivine appears eventually along the cotectic line, and clinopyroxene may crystallize at the eutectic point (Figure 9). However, to explain the crystallization of plagioclase from the liquidus, we speculate that the melt feeding the lenses correspond to a primitive melt stored at relatively high pressures. In its way to feed the melt lenses, it starts to crystallize olivine, which is dropped before the melt reach the lenses. The pressure decreasing due the melt upflowing can cause an expansion of the plagioclase field as a primary phase relative to olivine and clinopyroxene [*Kelemen et al.*, 1997; *Kelemen and Aharanov*, 1998], inducing the crystallization of plagioclase as the primary phase.

6.2. Origin of Microstructures and CPO in Anorthosites

[22] The evolution of the microstructures and CPO of plagioclases in the anorthosites from the upper gabbro section in the Oman ophiolite is controlled by two different, but interconnected aspects of the occurrence of these rocks. The first is the environment in which these anorthosites evolved, if they are related to the melt lens dynamics or to the subsidence of the axial magma chamber. In the case of melt lenses, we tried to separate the effect of four different possible mechanisms for the development and evolution of microstructures and CPO, including (1) crystal settling, (2) convection currents, (3) compaction of trapped melt, and (4) melt accumulation within the lens. On the other hand, the subsidence in the magma chamber and the floor of the melt lenses induces stretching and shearing of the anorthosites and gabbros formed within the melt lenses, and will be discussed separately.

6.2.1. Crystal Settling in the Floor of Melt Lenses

[23] In general, the textures of the anorthosites depend on the thickness of the anorthosite layers and lenses and on the local environment where they formed. Most of the thick layers of anorthosites have presumably settled directly in the floor of the melt lenses without other interference. The weak foliation associated with the absence of lineation (Figures 5a and 5b), together with the presence of rounded, millimeter-sized poikiloblasts of clinopyroxene suggests limited effect compaction in these rocks. Such field evidence is in agreement with the CPO of plagioclase (Figure 7a), which shows a weak preferred orientation of the (010) planes parallel to the foliation, with the [100] axis and poles to (001) with exactly the same distribution pattern along the foliation plane, with the maximum concentration of both axes lying in the same position of the pole figures.

[24] The density of parental basaltic magma responsible for the anorthosite generation varies between 2.64 and 2.95 g/cm^3 [*Sparks and Huppert*, 1984] whereas the density of a bytownite (An_{80}) is on average, 2.71 g/cm^3 [*Anthony et al.*, 1995], close to the density of 2.70 g/cm^3 adopted by *Liu and Lowell* [2009]. If the plagioclase is the first phase to crystallize in the studied anorthosites, it is expected that the parental magma was slightly enriched in Al_2O_3, and consequently less dense than the bytownite, allowing the plagioclase crystals around 1 to 2 mm long (the average dimension of the plagioclase tablets in the sample 07-2-OA-42, the best representative of this process) to sink toward the floor of the melt lenses instead of floating toward the roof. However, the sink of crystals and crystal settling on the floor of melt lenses is essentially a gravitational process, driven by the density difference between the liquid phase and the solid phase. The difference on the density between the solid and the liquid phases in the case of the anorthosites is relatively small, leading to a relatively slow sink of crystals. In addition, the crystal settling on the melt lenses floor does not occur in an organized form, and the resultant foliation and preferred orientation of plagioclase crystals is weak.

[25] The presence of normal zoning of plagioclase crystals, with An_{80} in the core and An_{60} in the rims suggest the crystallization under disequilibrium conditions, probably related to fast cooling. The fast cooling is also registered by the larger number of grains observed in thin section (Figure 5a) in comparison to the samples from higher depths. The absence of fluid inclusions in the cores or rims of the plagioclase in the zoned crystals suggest that the zoning was developed in a relatively dry environment, and not in a gas-saturated one, as typically occurs in the case of zoned plagioclases in volcanic rocks [e.g., *Anderson*, 1984]. Accumulation of residual melt in the anorthosites is testified by the poikilitic clinopyroxene. The presence of tiny inclusions of plagioclase within these clinopyroxenes corroborates

Figure 8. Crystallographic preferred orientation of plagioclase of (a–f) the steeply dipping anorthosites and (g–j) the anorthosites from the lower gabbro section for [100] axes and the poles to (010) and (001) planes. Pole figures plotted in the tectonic reference frame, with the vertical foliation aligned in the direction E-W and horizontal lineation also aligned in the direction E-W. Lower hemisphere, equal-area net, multiples of uniform distribution, MAD < 1.3°, inverse-log color scale.

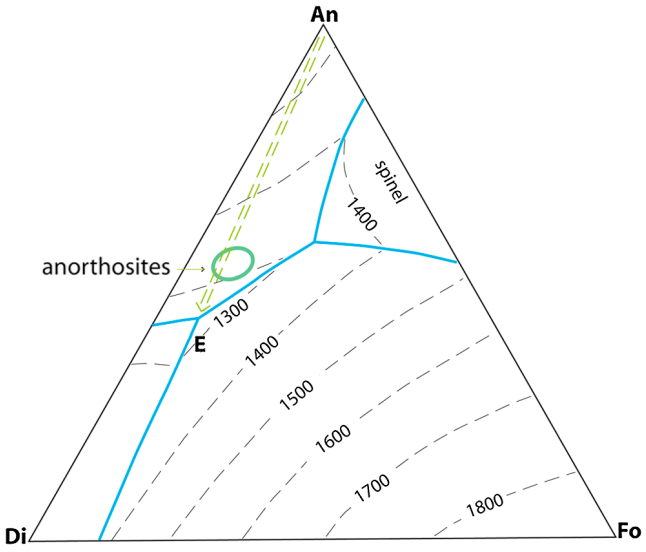

Figure 9. Phase equilibria diagram of the anorthite (An) diopside (Di) forsterite (Fo) system at room pressure to explain the initial crystallization of plagioclase at the floor of melt lens and progressive crystallization of diopside at the eutectic (E) point, following the evolution of crystallization, approximately marked by the arrow starting from An and pointing toward Di. Eventual crystallization of olivine may occur at the cotectic line An-Fo.

the crystallization order with plagioclase as an early nucleation. The lack of strong foliations in addition to the absence of lineation and the weak CPO of plagioclases suggest that pure crystal settling is not an important mechanism for fabric development, at least in special environment of the floor of the melt lenses.

6.2.2. Anorthosites Fabrics Related to Convection Currents

[26] Melt lens in general is the *locus* of a large thermal gradient, with temperatures grading from 1200°C at the bottom to 450°C at the base of the sheeted dike complex, with a very sharp thermal gradient (7°C–8°C/m) [*Nicolas et al.*, 2008]. Due to the scale of the lens (~2 km wide, 100 m thick) and cooling at the top, convection rolls should develop in order to thermally homogenize the system [*Liu and Lowell*, 2009]. The anorthosite layers assumed to relate convection are thin and usually interleaved with gabbros, given the rocks a typical banded aspect (Figures 4f and 6d). The first evidence of the activity of convection currents is the strong foliation of plagioclase developed in the first tens of meters below the sheeted dike complex. The presence of strong mineral lineations is another piece of evidence that favors the existence of convection in the melt lenses. In the field, lineations are strong and present well-organized patterns. In large (stable) melt lenses, they are parallel to the sheeted dike complex, whereas in retreating lenses, these lineations are normal to it [*Boudier and Nicolas*, 2011].

[27] Plagioclase crystals in these anorthosites are slightly larger in size and more elongated in the section normal to the foliation than the crystals statically settled on the floor of melt lenses. The strongest shape and crystallographic preferred orientation of plagioclase observed in this study (Figure 7b) and the "fluid" textures, together with synneusis features (Figure 5d) strongly suggest that the crystallization of these anorthosites occurred on a laminar magma flow [*Vance*, 1969], as expected from the effect of convection currents. In addition, the development of such a strong shape orientation can only be conceived if there was a large amount of melt present in the system, for the deformation operate by suspension flow. The increase in crystallinity of the mush induces a moderate increase on the viscosity until a value of 60% crystals in the system, when the viscosity increases so rapidly that the convection dies out [e.g., *Liu and Lowell*, 2009]. Therefore, fluidal textures as observed in Figure 5c can only be developed in systems where crystal content is <60%. The dominance of chemically homogeneous plagioclase below the first tens of meters beneath the root zone of the sheeted dike complex suggests a relatively slow crystallization [e.g., *Anderson*, 1984]. The absence of large poikilitic crystals possibly results from the continuous dispersion of the magma by the convection currents.

[28] To illustrate the variation in viscosity with the increase proportion of the solid phase, we carried a simple modeling of the viscosity of the anorthositic magma using the approach of *Giordano et al.* [2008], assuming the whole rock composition to that of plagioclase crystals (An_{80}) of the sample 07-2-OA-45c3, which we assign as representative of the convection currents. From this initial calculation, the viscosity of the liquidus anorthositic magma is 1.63 Pa s at 1200°C. We then calculate the effective viscosities of the anorthositic magma with variable proportion of a solid phase (Φ), using the relation of *Roscoe* [1952], assuming spherical particles and uniform size distribution (Figure 10):

$$\eta = \eta_0(1 - 1.35\Phi)^{-2.5}$$

where η = effective viscosity and η_0 = "liquidus" viscosity of the magma at a given temperature. A numerical modeling carried out by *Mainprice* [1997] in order to constrain the volume of melt within the magma chamber using the velocities of compressional waves (Vp) at the axial magma chamber [*Hussenoeder et al.*, 1996] predicts 50%–70% of melt, which signifies that Φ could vary between 0.3 and 0.5 within the axial magma chamber. Taking the minimum value of Φ = 0.3 for the magma chamber melt lenses viscosity will be very low (~6 Pa s) and the plagioclase cloud affected by the convection currents will be able to develop quite strong fabrics and "fluidal" textures (Figure 5c) within the convection currents. In this case, plagioclase crystals dropped by a dense convection current would lead to the development of an initial shape preferred orientation in a melt-rich, undercompacted layer [*Liu and Lowell*, 2009]. The next convection current and the drop of a new cloud of crystals results in shearing and compaction of the first layer, inducing an increase on the shape preferred orientation on the crystal mush. At 10–30 m below the floor of the melt lenses, the mush is compacted and very well oriented.

6.2.3. Geometry of Convection

[29] As a consequence of convection currents, the anorthosites develop a strong crystallographic preferred orientation characterized by the concentration of (010) planes parallel to the convection flow plane and the concentration [100] axes parallel to the lineation. In general, the lineation (flow direction) and consequently the strong concentration

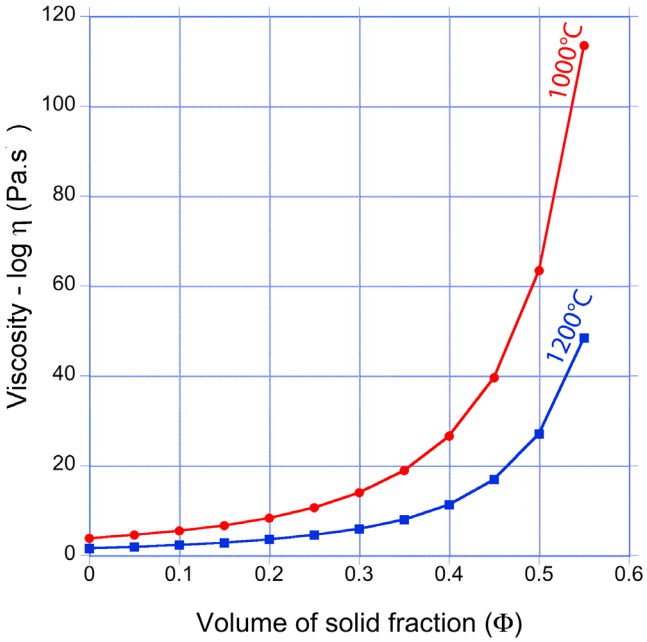

Figure 10. Graphic showing the variation of viscosity of an anorthositic magma at 1200°C and 1000°C with the increase in volume of the solid particles, calculated from the relation of *Roscoe* [1952]. Initial viscosities (Φ = 0) based on the composition given in the Table 2 and calculated through the method of *Giordano et al.* [2008] are 1.62 Pa s at 1200°C and 3.82 Pa s at 1000°C.

of plagioclase [100] axes in a laminar flow is normal to the axis of convection rolls. The lineations measured in the field are parallel or at low angle to the sheeted dikes complex in large melt lenses, but more or less normal to the ridge axis in retreating ones [*Nicolas and Boudier*, 2011]. As the sheeted dikes orientation is parallel to the to the ridge axis, then axis of convection rolls will be normal to the ridge axis in large and stable melt lenses, but parallel to the ridge axis in the retreating (unstable) ones. Considering the relationships between the (010) planes and [100] axis of plagioclase in relation to the convection flow plane and direction, then the maximum concentration of poles to (001) indicates approximately the orientation of the axes of the convection rolls.

[30] As the maximum of [100] in the stable melt lens convection currents is parallel to the sheeted dikes, there is no single rotation of plagioclase crystals capable to maintain the compatibility between flow plane and flow direction during the subsidence of the flat-lying lens floor (Figure 11a). However, in the case of unstable melt lenses, where the lineation tends to rotate to a position normal to the axial ridge, a rotation of the plagioclase crystals around the poles of (001) can maintain the compatibility relationship between foliations and lineations in the transition from the floor of the lens to the subsidence (Figure 11b). This means that when an anorthosite developed in stable melt lens subside, its previous fabric is obliterated by subsidence. We conclude that the flow related to convection currents is a very efficient mechanism to developed strong fabrics in anorthosites within the melt lens.

6.2.4. The Effect of Compaction in the Convection Current-Related Anorthosites

[31] The principal evidence of the effects of compaction is that the anorthosite layers tend to become totally monomineralic with depth. In other words, the poikilitic melt pockets where clinopyroxene and opaque minerals are observed have been squeezed. The CPO of plagioclase is also different (Figure 7c). In the specimen attributed to the effect of convection currents, the [100] axes are strongly concentrated around the lineation of the reference frame, but when the effect of compaction is also taken into account, these axes tend to be distributed along a continuous girdle parallel to the foliation. A similar effect is observed in the pole figures of the poles to (001) planes. If the melt is progressively "squeezed out" from the system with the progressive dip of the anorthosite layers due the subsidence, then the deformation of the crystal mush will become more and more difficult. It is likely that the first melt to be expelled was mainly the liquid trapped in the melt pockets and that the melt films along the plagioclase boundaries are probably largely preserved due the surface energy. The remaining melt along the interfaces allowed a certain degree of liberty and rotation of the axes [100] and poles to (001) around the poles of (010), with the consequent development of girdle-type CPOs for these two crystallographic axes. Once frozen due to drift outside the melt lens, both the CPO of [100] axes and (001) develop girdles, and no point-maximum CPOs are attributed to convection. As a consequence, some of the anorthosites may experience localized deformation by development of oblique twinning and dissolution/melting along grain boundaries, as observed in the Figures 5e and 6e.

6.2.5. The Effect of Melt Accumulation (Uncompacted Type)

[32] The melt accumulation occurs locally in the form of anorthosite spots. In addition to the weak foliation and the absence of lineation, the relatively weak CPOs and the large poikilitic clinopyroxenes and ilmenite preserved in these rocks, these places seem to have been preserved of the deformation caused by compaction. On the other hand, the melt itself could be responsible for an interesting modification on the plagioclase shape, that lead to an unusual CPO pattern of plagioclase. As evidenced by the microstructures (Figures 5g and 5h, sample 07-2-OA-41g), the plagioclase crystals depart from the normal tabular shape and are thicker than the crystals observed in most of the samples related to the melt lenses, assuming a prismatic shape. We do not know for sure the processes that control the thickening of crystals in these anorthosites but we can speculate that is related to the effect of anisotropy of free surface energy in different crystallographic planes, in addition to the space between crystals allowing the melt accumulation.

[33] Despite the lack of quantitative evaluation of the surface energy for different crystallographic planes of plagioclase single crystals, it is reasonable to assume that melt distribution in plagioclase crystals will have an anisotropic behavior due variations on the interface energies caused by variations on the atomic bounds in different planes of plagioclase. As an example of the crystallographic-controlled anisotropy of plagioclase crystal surfaces, the dissolution of albite is relatively faster along the (010) planes than (001) planes due the anisotropy of distribution between Al-O-Si

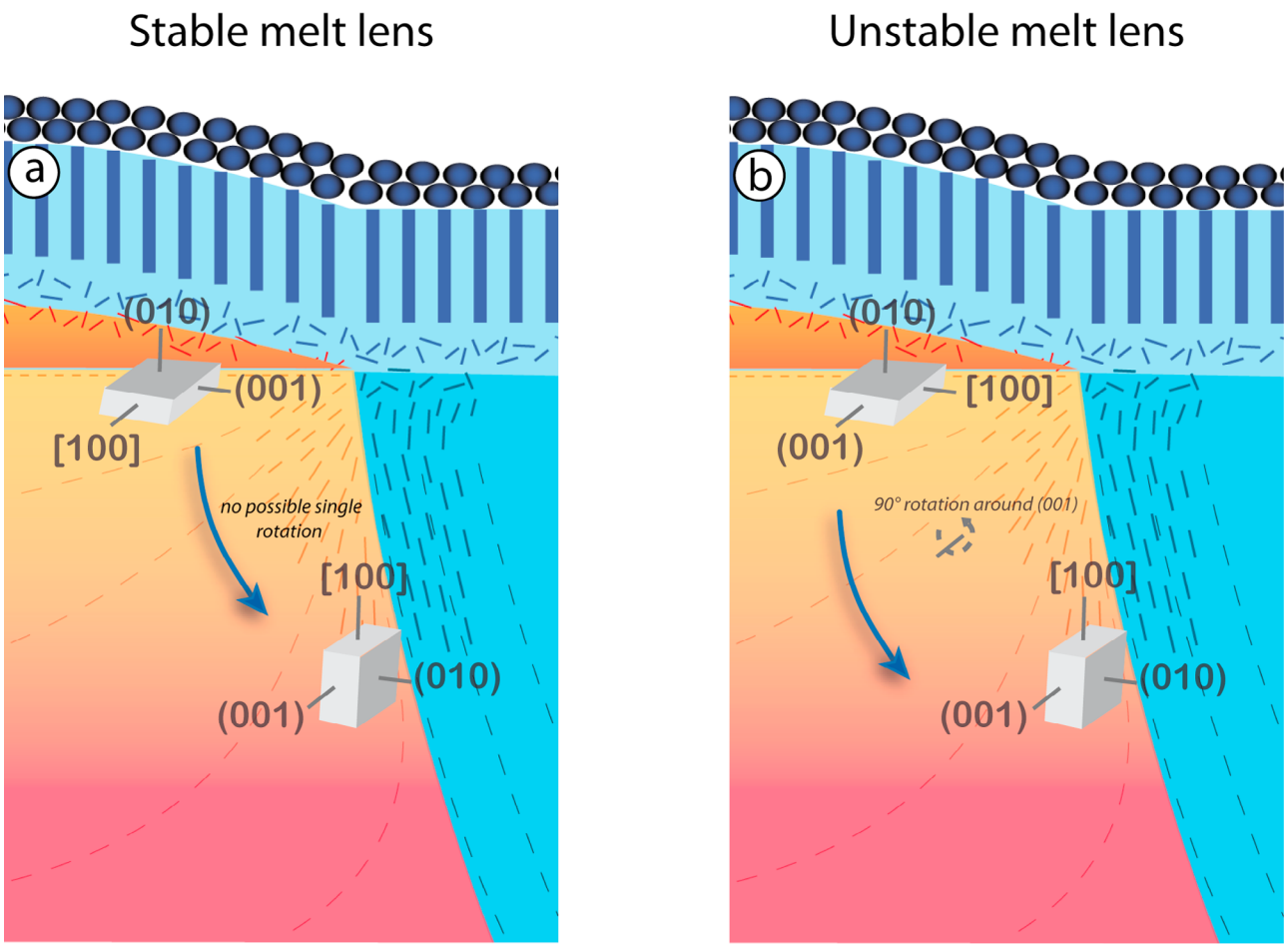

Figure 11. Schematic diagram showing the orientation of plagioclase crystals within the melt lenses (upper crystals) based on the CPO and the geometrical relationships between flow plane, flow direction, and convection rolls direction for (a) stable and (b) unstable melt lenses. The orientation of [100] marks the flow direction. Note that they are in different positions for each case. In the case of stable melt lens, there is no possible single rotation capable to maintain the compatibility between flow plane and direction at the triple junction from the orientation acquired from the flow in the melt lenses to the subsidence. However, a rotation of 90° around the pole of (001) of plagioclase maintains this compatibility in the case of unstable melt lenses, in which the lineation (and consequent concentration of [100]) is normal to the sheeted dikes direction.

and Si-O-Si bonds within its structure [*Arvidson et al.*, 2004]. The energy along any interface solid-liquid result from bonding mismatches along the fluid-crystal interface and its magnitude depends on the atomic structure of the interface, which is directly dependent to its orientation in relation to the crystallographic lattice [*Laporte and Watson*, 1995]. As described by *Spry* [1969], interfaces with dense atomic packing have low interfacial energy. In the case of studied anorthosites, we can postulate that the accumulation of melt occurs preferentially along the (010) planes, as observed in the microstructure. The melt accumulation leads to the thickening of crystals approximately in the direction of the pole of (001) and consequent decrease in the aspect ratio between the (010) and (001) axes of plagioclase. With a lower aspect ratio and the shapes resembling more a rod-shaped crystal, a rotation around the [100] axes of the plagioclase crystals becomes possible and explain the interchange between the (010) and (001) planes parallel to the weak foliation of these rocks (Figure 7c).

6.3. Anorthosites Fabrics Related to Subsidence

[34] The anorthosites related to the subsidence of the magmatic chamber recorded a new step of deformation to the already complicated history in the melt lenses due to the subsidence. The anorthosites that occupy the internal parts of the lens floor reach the magma chamber walls at great depths during the subsidence, in comparison to gabbros deposited near the limit of the melt lens. Due the long-standing time of deformation until they reach the magma chamber walls, the crystal mush is more susceptible to develop strong foliations. This explains the progressive variation in the microstructures and CPO in the Figures 6 and 8. Just below the root zone of the sheeted dike complex, the magmatic foliation is weak and no lineation is observed. Plagioclase crystals are small with low aspect

ratio and highly zoned, suggesting a rapid cooling under unstable conditions. This results from the short residence of these rocks until they reach the chamber walls. The development of foliation and consequent plagioclase CPO is progressive due the drifting process. With increasing depth, the foliation is more pronounced, and at depths around 50 m from the RZSDC, both the foliation and the plagioclase CPO are well developed as a result from increasing strain. Poikilitic clinopyroxene disappears progressively and with increasing depth, it crystallizes in tabular shape. Zoned plagioclase crystals also disappear due slower cooling. Impingement features begin to appear. They indicate partial dissolution of some plagioclase crystals, a process allowing further flow by suspension [*Nicolas and Ildefonse*, 1996]. With increasing depth, there is also an increase of the J index in the studied samples with steep foliation, starting with values around 2 just below the sheeted dike complex and reaching values of almost 9 at depths of 750 m. Increase of the fabric strength downsection is probably controlled by increasing flow and recrystallization. In the steep-dipping anorthosites, the (010) planes of plagioclase are parallel to the subsidence flow plane, and the generally plunging lineation and the maximum concentration of [100] axis marks the flow direction during the subsidence of the magmatic chamber. The increase in fabric strength is also expressed by the distribution patterns of poles to (010), whose concentration becomes stronger with depth, and seem to work as a rotation axis to [100] and (001), usually distributed as girdles.

6.4. Lower Crust Anorthosites

[35] The origin of the lower crustal anorthosites is problematic, mainly because part of these rocks are derived by subsidence from the floor of melt lens, but some are clearly intrusive in the layering of the gabbros. The later case implies that the anorthosites may derive from a melt circulating in the magma chamber through a thick crystal mush of gabbroic composition. The microstructures and CPO in the anorthosites from the lower crust near Moho record the high-temperature magmatic fabric, with a dominant mosaic texture. The anorthosites still preserve thick tabular, aligned crystals probably related to the older magmatic fabric of these rocks. Magmatic twins such as albite, pericline (and possibly Carlsbad) are well preserved, and do not show any evidence of bending. In addition, there is no evidence of activation of plasticity mechanisms in these rocks, such as abundant undulose extinction and subgrain boundaries. The presence of plagioclase crystal preferred orientation is therefore related to magmatic flow of a possibly thick crystal mush, without solid-state flow. The CPO of the specimen 95-OA-165a and 89-OA-17 (Figures 8g and 8h) clearly preserve the typical magmatic flow CPO, with the (010) poles parallel to Z and the [100] axes and (001) poles distributed along the foliation. The samples 07-2-OA-37 and 07-2-OA-37b (Figures 8i and 8j) on the other hand, show CPO patterns with concentration of both (010) and (001) poles parallel to the pole of the foliation, with [100] axes distributed along the foliation plane. In general, plagioclase crystals in igneous rocks with mosaic (or foam) textures have (010) and (001) dominant crystallographic planes and elongation along the [100] axis [*Smith and Brown*, 1988], forming crystals intermediate between tabular and prisms. The CPOs with the poles of (010) and (001) parallel to Z are then explained by an interchange between these planes parallel to the foliation, with a dominance of (010) over (001), as noticed in the relative concentration of these planes in the pole figures (Figures 8i and 8j). This is also corroborated by the microstructures, where the crystals with albite twin in the XZ section are always tabular over (010), whereas the crystals where the twins do not appear in this section tend to be tabular in (001), and the albite twins appear in the sections normal to both foliation and lineation (YZ) or parallel to the foliation (XY) [*Mainprice and Münch*, 1993]. The predominance of curved grain boundaries in these rocks indicates that the dominant mechanism of recrystallization in the studied anorthosites is grain boundary migration [*Nicolas and Poirier*, 1976; *Urai et al.*, 1986] (Figure 6g), and this process may have contributed to the fabric modification. The presence of triple junctions with dihedral angles of 120° also suggest that annealing took place after the deformation ceased (Figure 6h). Considering a solidus temperature for anorthosites ≤1200°C and the lack of indicative features of the presence of fluids (e.g., fluid inclusions, etc), the grain boundary migration recrystallization occur at ~1200°C. In such a situation, migration of boundaries is extensive and not limited to "bulging" features.

7. Conclusions

[36] In this contribution, we have analyzed the microstructures and orientation of fifteen samples of anorthosites from the Oman ophiolite. Eleven of them concern of bands interlayered in the upper gabbros. The anorthosite swarms in the upper gabbro section appear immediately below the root zone of the sheeted dike complex and their study provided information on the functioning of melt lenses and axial magma chamber subsidence in fast spreading ridges. In addition, four samples of layered and foliated anorthosites belonging to the lower gabbro section were also studied to understand their origin and the development of magmatic flow microstructures under high temperatures.

[37] In Nakhl (Figure 1b) the foliation in gabbros and anorthosites is flat lying and appears just a few meters below the sheeted dike complex. These anorthosites did not subside and record the dynamic processes of the melt lenses. In these rocks, we detected the role of four different processes responsible by the observed microstructures and CPO. Crystal settling in the lenses floor, driven by the density difference between the liquid phase and the plagioclase crystals usually produces weak foliations, no lineation and weak CPO. The anorthosites that were deposited on the lens floor by the activity of convection currents develop strong foliations and lineations, fluidal textures with strong shape preferred orientation strong CPOs and synneusis microstructures. Together, these evidences suggest that the fabric was developed in a laminar suspension flow, as expected in an environment under active convection currents. In this case, the planes (010) of plagioclase mark the flow plane of the convection currents, whereas the [100] axes characterize the flow direction and the poles of (001) are subparallel to the axis of convection rolls. The main effect of compaction in the anorthosites deposited from convection currents is to expel the melt from the crystal mush. As a result, deformation becomes difficult and explains the distribution of

[100] axes as girdles, and not as point-maximum parallel to X. The accumulation of melt in uncompacted isolated pockets induced the crystallization of prismatic-shaped plagioclases, possibly due the spacing between crystals and due the anisotropy of surface energy. This explains the anomalous CPO where both (010) and (001) plagioclase planes are parallel to the foliation in the pole figures.

[38] In Jabal Dihm (Figure 1) of the Wadi Tayin massif, the effect of subsidence is immediately recorded 10 m below the root zone of the sheeted dikes complex and it is expressed by the development of a dipping foliation and lineation rapidly steepening with depth. The development of these structures together with plagioclase CPO, is progressive, reflecting the increasing strain conditions down in the section. The degree of development of the microstructures and CPO in the anorthosites is directly related to their distance on the floor from the center of the melt lenses before subsidence process started. Therefore, anorthosites deposited in the melt lenses close to its wall do not subside substantially below the sheeted dike complex before they crystallize. In this case, the CPO is weak. On the other hand, anorthosites from central parts of the floor have a longer travel inside the axial magma chamber until they reach its wall and develop strong foliations and CPOs.

[39] The microstructures in the lower crust anorthosites are partially modified, and the aggregates have mosaic (or foam) textures typical of equilibrium under high temperatures, but no evidence of activation of solid-state deformation. The magmatic flow CPO is preserved, and variations on fabric patterns, such as the occurrence of (010) and (001) planes parallel to the foliation is explained by variations on the plagioclase crystal shape forming foam textures the interchange between these two planes in parallelism with the flow plane.

[40] **Acknowledgments.** The authors would like to thank Christophe Nevado for the preparation of high-quality polished EBSD thin sections and Benoît Ildefonse and David Mainprice for the discussions and tips of magma viscosity and plagioclase orientation. We are also grateful to David Mainprice for providing the latest versions of the programs for pole figures plotting and calculations of J index. The authors are grateful to the two anonymous reviewers and the Associate Editor for the thoughtful comments and criticisms that helped to improve the final version of the paper. L.F.G.M. thanks the French Agence Nationale de la Recherche for the postdoctoral fellowship, project CRYSTALTEX.

References

Anderson, A. T., Jr. (1984), Probable relations between plagioclase zoning and magma dynamics, Fuego Volcano, Guatemala, *Am. Mineral.*, *69*, 660–676.

Anthony, J. W., R. A. Bideaux, K. W. Bladh, and M. C. Nichols (1995), *Handbook of Mineralogy*, vol. 2, Min. Data Publ., Tucson, Ariz.

Arvidson, R. S., M. S. Beig, and A. Luttge (2004), Single-crystal plagioclase feldspar dissolution rates measured by vertical scanning interferometry, *Am. Mineral.*, *89*, 51–56.

Bédard, J. H. (1991), Cumulate recycling and crustal evolution in the Bay of Islands ophiolite, *J. Geol.*, *99*, 225–249, doi:10.1086/629486.

Boudier, F., and A. Nicolas (2011), Axial melt lenses at oceanic ridges—A case study in the Oman Ophiolite, *Earth Planet. Sci. Lett.*, doi:10.1016/j.epsl.2011.01.029, in press.

Boudier, F., A. Nicolas, and B. Ildefonse (1996), Magma chambers in the Oman ophiolite: Fed from the top or from the bottom?, *Earth Planet. Sci. Lett.*, *144*, 239–250, doi:10.1016/0012-821X(96)00167-7.

Boudreau, A. E. (1987), Pattern formation during crystallization and the formation of fine-scale layering, in *Origin of Igneous Layering*, edited by I. Parson, *NATO ASI Ser., Ser. C*, *196*, 453–471.

Bunge, H.-J. (1982), *Texture Analysis in Materials Science*, Butterworths, London.

Feinberg, J. M., H.-R. Wenk, G. R. Scott, and P. R. Renne (2006), Preferred orientation and anisotropy of seismic and magnetic properties in gabbronorites from the Bushveld layered intrusion, *Tectonophysics*, *420*, 345–356, doi:10.1016/j.tecto.2006.03.017.

Giordano, D., J. K. Russell, and D. B. Dingwell (2008), Viscosity of magmatic liquids: A model, *Earth Planet. Sci. Lett.*, *271*, 123–134, doi:10.1016/j.epsl.2008.03.038.

Hussenoeder, S. A., J. A. Collins, G. M. Kent, R. S. Detrick, and the TERA Group (1996), Seismic analysis of the axial magma chamber reflector along the southern East Pacific Rise from conventional reflection profiling, *J. Geophys. Res.*, *101*, 22,087–22,105, doi:10.1029/96JB01907.

Irvine, T. N. (1987), Layering and related structures in the Duke Island and Skaergard intrusions: Similarities, differences and origins, in *Origin of Igneous Layering*, edited by I. Parson, *NATO ASI Ser., Ser. C*, *196*, 185–245.

Kelemen, P. B., and E. Aharanov (1998), Periodic formation of magma fractures and generation of layered gabbros in the lower crust beneath oceanic spreading ridges, in *Faulting and Magmatism at Mid-Ocean Ridges*, *Geophys. Monogr. Ser.*, vol. 106, edited by W. R. Buck et al., pp. 267–289, AGU, Washington, D. C.

Kelemen, P. B., K. Koga, and N. Shimizu (1997), Geochemistry of gabbro sills in the crust-mantle transition zone of the Oman ophiolite: Implications for the origin of the oceanic lower crust, *Earth Planet. Sci. Lett.*, *146*(3–4), 475–488, doi:10.1016/S0012-821X(96)00235-X.

Kent, G. M., A. J. Harding, J. A. Orcutt, R. S. Detrick, J. C. Mutter, and P. Buhl (1994), Uniform accretion of oceanic crust south of the Garret transform at 14°15′S on the East Pacific Rise, *J. Geophys. Res.*, *99*, 9097–9116, doi:10.1029/93JB02872.

Lamoureux, G. (1999), Structure des gabbros de l'ophiolite d'Oman: Caractérisation physique des chambres magmatiques des dorsales océaniques rapides, Ph.D. thesis, 135 pp., Univ. Montpellier II, Montpellier, France.

Laporte, D., and E. B. Watson (1995), Experimental and theoretical constraints on melt distribution in crustal sources: The effect of crystalline anisotropy on melt interconnectivity, *Chem. Geol.*, *124*, 161–184, doi:10.1016/0009-2541(95)00052-N.

Liu, L., and R. P. Lowell (2009), Models of hydrothermal heat output from a convecting, crystallizing, replenished magma chamber beneath an oceanic spreading center, *J. Geophys. Res.*, *114*, B02102, doi:10.1029/2008JB005846.

Mainprice, D. (1997), Modelling the anisotropic seismic properties of partially molten rocks found at mid-ocean ridges, *Tectonophysics*, *279*, 161–179, doi:10.1016/S0040-1951(97)00122-4.

Mainprice, D., and P. Münch (1993), Quantitative texture analysis of an anorthosite—Application to thermal expansion, Young's modulus and thermal stresses, *Textures Microstruct.*, *21*, 79–92, doi:10.1155/TSM.21.79.

Morse, S. A. (1980), *Basalts and Phase Diagrams: An Introduction to the Quantitative Use of Phase Diagrams in Igneous Petrology*, 493 pp., Springer, New York.

Nicolas, A., and F. Boudier (2011), Structure and dynamics of ridge axial melt lenses in the Oman ophiolite, *J. Geophys. Res.*, *116*, B03103, doi:10.1029/2010JB007934.

Nicolas, A., and B. Ildefonse (1996), Flow mechanisms and viscosity in basaltic magma chambers, *Geophys. Res. Lett.*, *23*, 2013–2016, doi:10.1029/96GL02073.

Nicolas, A., and J.-P. Poirier (1976), *Crystalline Plasticity and Solid State Flow in Metamorphic Rocks*, 444 pp., John Wiley, New York.

Nicolas, A., F. Boudier, J. Koepke, L. France, B. Ildefonse, and C. Mevel (2008), Root zone of the sheeted dike complex in the Oman ophiolite, *Geochem. Geophys. Geosyst.*, *9*, Q05001, doi:10.1029/2007GC001918.

Nicolas, A., F. Boudier, and L. France (2009), Subsidence in magma chamber and the development of magmatic foliation in Oman ophiolite gabbros, *Earth Planet. Sci. Lett.*, *284*, 76–87, doi:10.1016/j.epsl.2009.04.012.

Pallister, J. S., and C. A. Hopson (1981), Samail ophiolite plutonic suite: Field relations, phase variation, cryptic variation and layering, and a model of a spreading ridge magma chamber, *J. Geophys. Res.*, *86*, 2593–2644, doi:10.1029/JB086iB04p02593.

Prior, D. J., et al. (1999), The application of electron backscatter diffraction and orientation contrast imaging in the SEM to textural problems in rocks, *Am. Mineral.*, *84*, 1741–1759.

Randle, V. (1992), *Microtexture Determination and Its Applications*, 174 pp., Inst. of Mater., Miner. and Min., London.

Randle, V., and O. Engler (2000), *Introduction to Texture Analysis: Macrotexture, Microtexture and Orientation Mapping*, 388 pp., CRC Press, London.

Roscoe, R. (1952), The viscosity of suspensions of rigid spheres, *Br. J. Appl. Phys.*, *3*, 267–269, doi:10.1088/0508-3443/3/8/306.
Smith, J. V., and W. L. Brown (1988), *Feldspar Minerals*, vol. 1, 828 pp., Springer, Berlin.
Sparks, R. S. J., and H. E. Huppert (1984), Igneous petrology: Old magma chambers replenished by new ideas, *Nature*, *312*, 200.
Spry, A. (1969), *Metamorphic Textures*, 350 pp., Pergamon, Oxford, U. K.
Tommasi, A., D. Mainprice, G. Canova, and Y. Chastel (2000), Viscoplastic self-consistent and equilibrium-based modeling of olivine lattice preferred orientations: Implications for the upper mantle seismic anisotropy, *J. Geophys. Res.*, *105*, 7893–7908, doi:10.1029/1999JB900411.
Urai, J. L., W. D. Means, and G. S. Lister (1986), Dynamic recrystallization of minerals, in *Mineral and Rock Deformation: Laboratory Studies*, *Geophys. Monogr. Ser.*, vol. 36, edited by B. E. Hobbs and H. C. Heard, pp. 161–199, AGU, Washington, D. C.
Vance, J. A. (1969), On synneusis, *Contrib. Mineral. Petrol.*, *24*, 7–29, doi:10.1007/BF00398750.

F. Boudier and A. Nicolas, Géosciences Montpellier, UMR, CNRS 5243, Université Montpellier 2, Place Eugène Bataillon, Batîment 22, F-34095 Montpellier CEDEX 05, France.
L. F. G. Morales, Section 3.2, Deutsches GeoForschungsZentrum, Telegrafenberg, D-14473 Potsdam, Germany. (luiz_grafulha@yahoo.com.br)